

Efficient Parameter Estimation in Biochemical Pathways: Overcoming Data Limitations with Constrained Regularization and Fuzzy Inference

Abhisek Bakshi¹, Souvik Sengupta², Rajat K. De^{3*}, and Abhijit Dasgupta^{4,5*}

¹Department of Research and Development, Michelin India Private Limited, Pune, MH 411014, India, Email: abhisek.bakshi@michelin.com;

²Department of Computer Science and Engineering, Aliah University, Kolkata, WB 700156, India, Email: ssg@aliah.ac.in;

³Machine Intelligence Unit, Indian Statistical Institute, Kolkata, WB 700108, India, Email: rajat@isical.ac.in;

⁴Department of Structural Biology, St. Jude Children's Research Hospital, Memphis, TN 38105, USA, Email: Abhijit.Dasgupta@stjude.org;

⁵Department of Computer Science and Engineering, SRM University AP, Guntur, AP 522240, India, Email: abhijit.d@srmmap.edu.in

Abstract

In analytical modeling for biochemical pathways, precisely determining unknown parameters is paramount. Traditional methods, reliant on experimental time course data, often encounter roadblocks—limited accessibility and variable quality—that can significantly impact the algorithm's performance. In this study, we address these hurdles by unveiling a groundbreaking parameter estimation technique, Constrained Regularized Fuzzy Inferred Extended Kalman Filter (CRFIEKF). This innovative approach eliminates the need for experimental time-course measurements and capitalizes on the existing imprecise relationships among the molecules within the network. Our proposed framework integrates a Fuzzy Inference System (FIS) block to encapsulate these approximated relationships. To fine-tune the estimated parameter values, we employ Tikhonov regularization. The selection of Tikhonov regularization and Gaussian membership functions was based on the Mean Squared Error (MSE) values observed during the parameter estimation process, contrasting our results with those of previous studies.

We rigorously tested the proposed approach across various pathways, from the glycolytic processes in mammalian erythrocytes and yeast cells to the intricate JAK/STAT and Ras signaling pathways. The results were impressive, showing a significant similarity (p -value < 0.001) to the outcomes of specific prior experiments. The dynamics of the biochemical networks normalized within the $[0, 1]$ range mirrored the transient behavior ($MSE < 0.5$) of both *in vivo* and *in silico* results from previous studies. In conclusion, our findings highlight the effectiveness of CRFIEKF in estimating the kinetic parameter values without prior knowledge of experimental data within a biochemical pathway in the state-space model. The proposed method underscores its potential as a game-changer in biochemical pathway analysis.

Supplementary information: Supplementary data are available at [github](#).
Code availability: The code and sample data for the estimation technique is available at [github](#).

Keywords: State space model, Fuzzy inference system, Tikhonov regularization, Convex quadratic programming, ill-posed problem, Kalman filter.

*For all correspondence, direct it to Rajat K. De, Ph.D., Machine Intelligence Unit, Indian Statistical Institute, Kolkata, WB 700108, India, Email: rajat@isical.ac.in or Abhijit Dasgupta, Ph.D., Department of Computer Science and Engineering, SRM University AP, Guntur, AP 522240, India, Email: abhijit.d@srmmap.edu.in

1. Algorithm

Algorithm 1.1: CRFIEKF algorithm (L1 regularization): Assuming there are ‘m’ number of state components in the extended biochemical pathway. Besides, we consider the ‘n’ number of approximated measurements available to us.

```

Data:  $\hat{\mathbf{x}}_0^{' +}, \widehat{\mathbf{W}}_0^+, \mathcal{R}_\epsilon, N_\tau$ 
Result:  $\mathbf{k}$ 

1  $D \leftarrow -I$ 
2  $\vec{d} \leftarrow 1$ 
3  $iter \leftarrow 0$ 
4  $time \leftarrow [0 : 0.002 : 10]$ 
5 while  $p \leq limit$  do
6    $\mathcal{J}_p^f \leftarrow Jacobean(time(p), \hat{\mathbf{x}}_p^{' +})$ 
7    $\dot{\hat{\mathbf{x}}} \leftarrow f(\hat{\mathbf{x}}^{'}, \mathbf{u}) \quad where \quad \hat{\mathbf{x}}'(t_{p-1}) \leftarrow \hat{\mathbf{x}}_{p-1}^{' +}$ 
8    $\hat{\mathbf{x}}_p^{'} \leftarrow \hat{\mathbf{x}}'(t_p)$ 
9    $\dot{\widehat{\mathbf{W}}} \leftarrow P(\mathcal{J}_p^f, \mathbf{W}, \mathcal{Q}) \quad where \quad \mathbf{W}(t_{p-1}) \leftarrow \widehat{\mathbf{W}}_{p-1}^+$ 
10   $\widehat{\mathbf{W}}_p^- \leftarrow \mathbf{W}(t_{p-1})$ 
11   $\mathcal{G}_p \leftarrow \widehat{\mathbf{W}}_p^- \mathcal{J}_p^{hT} (\mathcal{J}_p^h \widehat{\mathbf{W}}_p^- \mathcal{J}_p^{hT} + \mathcal{R})^{-1}$ 
12   $\mathbf{z}_p \leftarrow FIS(\hat{\mathbf{x}}_p^{' -})$ 
13   $\hat{\mathbf{x}}_p^{' +} \leftarrow \hat{\mathbf{x}}_p^{' -} + \mathcal{G}_p(\mathbf{z}_p - h(\hat{\mathbf{x}}_p^{' -}))$ 
14   $\widehat{\mathbf{W}}_p^+ \leftarrow (I - \mathcal{G}_p \mathcal{J}_p^h) \widehat{\mathbf{W}}_p^- (I - \mathcal{G}_p \mathcal{J}_p^h)^T + \mathcal{G}_p \mathcal{R} \mathcal{G}_p^T$ 
15   $\widehat{\mathbf{W}}_{reg} \leftarrow \widehat{\mathbf{W}}_p^+$ 
16   $\hat{\mathbf{x}}_{reg} \leftarrow \hat{\mathbf{x}}_p^{' +}$ 
17  while  $\tau \leq N_\tau$  do
18     $\bar{\mathcal{H}} \leftarrow [\xi(1 \hat{\mathbf{x}}_p^{'}), \xi(2 \hat{\mathbf{x}}_p^{'}), \dots, \xi((m+n) \hat{\mathbf{x}}_p^{'})]$ 
19     $\mathcal{K}_{RFIEKF} \leftarrow \widehat{\mathbf{W}}_{reg} \bar{\mathcal{H}}^T (\bar{\mathcal{H}} \widehat{\mathbf{W}}_{RFIEKF} \bar{\mathcal{H}}^T + \mathcal{R}_\epsilon)^{-1}$ 
20     $\hat{\mathbf{x}}_{RFIEKF} \leftarrow (I - \mathcal{K}_{reg} \bar{\mathcal{H}}) \hat{\mathbf{x}}_{RFIEKF}^{'}$ 
21     $\widehat{\mathbf{W}}_{RFIEKF} \leftarrow (I - \mathcal{K}_{RFIEKF} \bar{\mathcal{H}}) \widehat{\mathbf{W}}_{RFIEKF}$ 
22  end
23   $\widehat{\mathbf{W}}_p^+ \leftarrow \widehat{\mathbf{W}}_{reg}$ 
24   $\hat{\mathbf{x}}_p^{' +} \leftarrow \hat{\mathbf{x}}_{reg}^{' +}$ 
25  if  $D \hat{\mathbf{x}}_p^{' +} \leq d$  then
26     ${}_c \hat{\mathbf{x}}_p^{' +} \leftarrow \vec{d} - D \hat{\mathbf{x}}_p^{' +}$ 
27     $cons \leftarrow Quadratic\_programming(\widehat{\mathbf{W}}_p^+, D, {}_c \hat{\mathbf{x}}_p^{' +})$ 
28     $\hat{\mathbf{x}}_p^{' +} \leftarrow \hat{\mathbf{x}}_p^{' +} + cons$ 
29  else
30    | Continue
31  end
32 end

```

Algorithm 1.2: CRFIEKF algorithm (Tikhonov regularization): Assuming there are ‘m’ Number of state components in the extended biochemical pathway. Besides, we consider the ‘n’ number of approximated measurements available.

Data: $\hat{\mathbf{x}}_0^{' +}, \widehat{\mathbf{W}}_0^+, \mathcal{R}, \lambda$
Result: \mathbf{k}

- 1 $D \leftarrow -I$
- 2 $\vec{d} \leftarrow 1$
- 3 $iter \leftarrow 0$
- 4 $time \leftarrow [0 : 0.002 : 10]$
- 5 **while** $p \leq limit$ **do**
- 6 $\mathcal{J}_p^f \leftarrow Jacobean(time(p), \hat{\mathbf{x}}_p^{' +})$
- 7 $\dot{\hat{\mathbf{x}}} \leftarrow f(\hat{\mathbf{x}}^{'}, \mathbf{u}) \quad where \quad \hat{\mathbf{x}}^{'}(t_{p-1}) \leftarrow \hat{\mathbf{x}}_{p-1}^{' +}$
- 8 $\dot{\hat{\mathbf{x}}}_p^{' -} \leftarrow \dot{\hat{\mathbf{x}}}(\mathbf{t}_p)$
- 9 $\widehat{\mathbf{W}} \leftarrow P(\mathcal{J}_p^f, \mathbf{W}, \mathcal{Q}) \quad where \quad \mathbf{W}(t_{p-1}) \leftarrow \widehat{\mathbf{W}}_{p-1}^+$
- 10 $\widehat{\mathbf{W}}_p^- \leftarrow \mathbf{W}(\mathbf{t}_{p-1})$
- 11 $\mathcal{G}_p \leftarrow \widehat{\mathbf{W}}_p^- \mathcal{J}_p^{h^T} (\mathcal{J}_p^h \widehat{\mathbf{W}}_p^- \mathcal{J}_p^h + \mathcal{R})^{-1}$
- 12 $\mathbf{z}_p \leftarrow FIS(\hat{\mathbf{x}}_p^{' -})$
- 13 $\hat{\mathbf{x}}_p^{' +} \leftarrow \hat{\mathbf{x}}_p^{' -} + \mathcal{G}_p(\mathbf{z}_p - h(\hat{\mathbf{x}}_p^{' -}))$
- 14 $\widehat{\mathbf{W}}_p^+ \leftarrow (I - \mathcal{G}_p \mathcal{J}_p^h) \widehat{\mathbf{W}}_p^- (I - \mathcal{G}_p \mathcal{J}_p^h)^T + \mathcal{G}_p \mathcal{R} \mathcal{G}_p^T$
- 15 $normal_matrix \leftarrow \mathcal{J}_p^{h^T} \mathcal{R}^{-1} \mathcal{J}_p^h + \widehat{\mathbf{W}}_p^+$
- 16 $cond \leftarrow Norm(normal_matrix) * Norm(inv(normal_matrix))$
- 17 **if** $cond \geq Threshold$ **then**
- 18 $\mathcal{G}_p^{RFIEKF} = \mathcal{J}_p^{h^T} \mathcal{R}^{-1} \mathcal{J}_p^h + \widehat{\mathbf{W}}_p^+ + \lambda \cdot \widehat{\mathbf{W}}_p^{+ -1}$
- 19 $\hat{\mathbf{x}}_p^{RFIEKF} = \hat{\mathbf{x}}_p^{' -} + \mathcal{G}_p^{RFIEKF}(\mathbf{z}_p - h(\hat{\mathbf{x}}_p^{' -}))$
- 20 $\widehat{\mathbf{W}}_p^{RFIEKF} = (I - \mathcal{G}_p^{RFIEKF} \mathcal{J}_p^h) \widehat{\mathbf{W}}_p^+$
- 21 $\hat{\mathbf{x}}_p^{' +} \leftarrow \hat{\mathbf{x}}_p^{RFIEKF}$
- 22 $\widehat{\mathbf{W}}_p^+ \leftarrow \widehat{\mathbf{W}}_p^{RFIEKF}$
- 23 **else**
- 24 | Continue
- 25 **end**
- 26 **if** $D \hat{\mathbf{x}}_p^{' +} \leq d$ **then**
- 27 $c \hat{\mathbf{x}}_p^{' +} \leftarrow \vec{d} - D \hat{\mathbf{x}}_p^{' +}$
- 28 $cons \leftarrow Quadratic_programming(\widehat{\mathbf{W}}_p^+, D, c \hat{\mathbf{x}}_p^{' +})$
- 29 $\hat{\mathbf{x}}_p^{' +} \leftarrow \hat{\mathbf{x}}_p^{' +} + cons$
- 30 **else**
- 31 | Continue
- 32 **end**
- 33 **end**

Table 1. Different mathematical symbols and their description

$\mathbf{x}, \mathbf{y}, \mathbf{u}$ and \mathbf{k}	Vectors representing input molecule expression/concentration levels, output molecule expression/concentration levels, concentration of external inputs and kinetic parameters respectively.
n'' and q	Number of molecules involved in the known approximate relationship in the biochemical pathway and Number of discrete time instant, respectively.
p	Index for the discrete time instant.
\mathbf{z}_p	Vectors representing measurement signal, evaluated using known approximated relationship among molecules involved in the biochemical pathway.
n, n', s and m and l	Dimension of $\mathbf{x}, \mathbf{y}, \mathbf{u}, \mathbf{k}$ and \mathbf{z}_p respectively.
i, j and l'	Index for \mathbf{x}, \mathbf{k} and \mathbf{z}_p involved in the biochemical pathway respectively.
\mathbf{x}'	State vector representing expression/concentration levels extended state space model of the biochemical pathway.
\mathbf{x}'_p	State vector representing expression/concentration levels extended state space model of the biochemical pathway at p^{th} time instant.
$\dot{\mathbf{x}}', \dot{\mathbf{k}}$	Derivatives of \mathbf{x}', \mathbf{k} respectively, with respect to time t .
w and v_p	Process noise and measurement noise at p^{th} time instant respectively .
\mathcal{Q} and \mathcal{R}	covariance matrix of w and v_p respectively .
$f(\cdot), h(\cdot)$, and $g(\cdot)$	Nonlinear functions corresponding to input, output, and approximate relationship among certain molecules of the extended state space model of the biochemical pathway, respectively.
j'	Index of the molecules involved in the known approximate relationship among specific molecules of \mathbf{x}'_p .
$c_{j'}' \text{ and } f_{j'}'$	Crisp and fuzzy value of the j' molecule $x_{j'}' \in \mathbf{x}'_p$ respectively.
$f\mathbf{x}'_p$	The fuzzy set corresponding to \mathbf{x}'_p .
$\underline{x}_{j'}', \mathcal{L}\underline{x}_{j'}', \mathcal{U}\underline{x}_{j'}' \text{ and } \mu_{\underline{x}_{j'}'}$	linguistic variable of $x_{j'}'$, set of linguistic values that $x_{j'}'$ can take, Universe of discourse of $\underline{x}_{j'}'$ and Gaussian membership function for $\underline{x}_{j'}'$ respectively.
ε and ρ	Center and width of the fuzzy set $f\mathbf{x}'_p$.
\mathcal{F}_r and r	Number of fuzzy rules and the Index of fuzzy rules.
z_p^r	r^{th} measurement signal at p^{th} time instant.
$r z_p^r$	Fuzzy value of z_p^r on applying r^{th} fuzzy rule.
j''	Index of the linguistic values $\in \mathcal{L}\underline{x}_{j''}$ for the fuzzy variable $f_{j''}$.
$\alpha_{j''}^r$	Firing strength of $r z_p^r$ based on r^{th} fuzzy rule.
\mathbf{W}	Error covariance matrix of CRFIEKF.
$\hat{\mathbf{x}}'^+$ and $\hat{\mathbf{x}}'^-$	a posteriori and a priori estimate respectively of $\hat{\mathbf{x}}$.
$\widehat{\mathbf{W}}^+$ and $\widehat{\mathbf{W}}^-$	a posteriori and a priori estimate respectively of error covariance matrix \mathbf{W} .
$\dot{\mathbf{x}}'$ and $\dot{\mathbf{W}}$	Time derivative of x' and \mathbf{W} respectively.
\mathcal{J}_p^f and \mathcal{J}_p^h	Jacobeian of $f(\cdot)$ and $h(\cdot)$ respectively.
\mathcal{G}_p and I	Kalman gain at p^{th} time instant and Identity matrix respectively.
λ, ϵ and \mathcal{R}_ϵ	regularization parameter, kinetic parameter measurement noise, and covariance matrix of ϵ , respectively.
N_τ	Number of iteration in L1 regularization algorithm.
\mathbf{N}_p	Normal matrix of Standard EKF equation.
$C(\mathbf{N}_p)$	Condition number of Normal matrix \mathbf{N}_p .
$\mathcal{G}_p^{RFIEKF}, \hat{\mathbf{x}}_p^{RFIEKF}$ and $\widehat{\mathbf{W}}_p^{RFIEKF}$	Tikhonov regularized Kalman gain, regularized state vector and regularized error covariance matrix respectively at p^{th} time instant.
$\hat{\mathbf{x}}_p^{CRFIEKF}$	Constraint Tikhonov regularized state vector at p^{th} time instant.
η and \varkappa	Number of constraints and state components of the extended state space model, respectively.
\mathbf{k}^{final} and \mathbf{x}^{final}	Final values of states and estimated parameter.

2. Parameter estimation of Generic branch pathway model (Jia et al., 2012)

We examined a generic branched pathway model (Jia et al., 2012) (depicted in Supplementary Figure 1) encompassing five molecules and fourteen associated kinetic parameters, with six of these parameters remaining unknown. To tackle this, we devised a Fuzzy Inference System (FIS) to capture well-established approximate relationships among these molecules, as indicated by activation and inhibition interactions in Supplementary Figure 1. Detailed reaction fluxes and the stoichiometric matrix are presented in Supplementary Tables 2-3.

To facilitate the application of CRFIEKF for parameter estimation, we inferred the known imprecise relationships based on expert knowledge. These relationships are outlined in Supplementary Tables 4-5. Subsequently, we employed the proposed method to estimate the unknown parameter values. The results revealed that the majority of the estimated parameter values (enumerated in Supplementary Table 6) closely align with previous findings (Jia et al., 2012; Voit and Almeida, 2004). The marginal differences between the estimated parameter values in our approach and those from prior methods underscore the effectiveness of our proposed technique. A visual representation of the comparison is presented in Supplementary Figure 2.

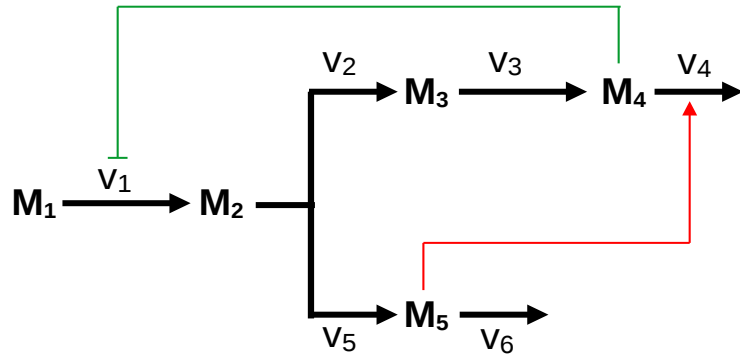


Figure 1. A generic branched pathway presented in Jia et al. (Jia et al., 2012)

Table 2. Reaction equations contains the equations of reaction fluxes presented in Jia et al. (Jia et al., 2012)

1. $v_1 = \frac{\gamma_1 M_1}{M_3^{f_{13}}}$
2. $v_2 = \gamma_2 M_2^{f_{21}}$
3. $v_3 = \gamma_3 M_3^{f_{32}}$
4. $v_4 = \gamma_4 M_4^{f_{43}} M_5^{f_{44}}$
5. $v_5 = \gamma_5 M_2^{f_{51}}$
6. $v_6 = \gamma_6 M_5^{f_{64}}$

Table 3. It contains the stoichiometric matrix associated with the reactions from the generic branch pathway model(Jia et al., 2012) under consideration.

	v1	v2	v3	v4	v5	v6
M1	1	-1	0	0	-1	0
M2	0	1	-1	0	0	0
M3	0	0	1	-1	0	0
M4	0	0	0	0	1	-1

Table 4. IF-THEN rule base for FIS to capture fuzzy relationship between M_2 , M_4 & M_3

IF (M_2 & M_4)		Then M_3
M_2	M_4	M_3
LOW	LOW	MEDIUM
LOW	MEDIUM	MEDIUM
LOW	HIGH	LOW
MEDIUM	LOW	MEDIUM
MEDIUM	MEDIUM	MEDIUM
MEDIUM	HIGH	LOW
HIGH	LOW	MEDIUM
HIGH	MEDIUM	LOW
HIGH	HIGH	HIGH

Table 5. IF-THEN rule base for FIS to capture fuzzy relationship between M_3 & M_1

IF M_3		Then M_1
M_3		M_1
LOW		HIGH
MEDIUM		MEDIUM
HIGH		LOW

Table 6. The list of parameter values of the generic branch pathway model(Jia et al., 2012). Here, we estimate seven parameter values (represented as “Estimated”) of the pathway under consideration. Rest of the parameter values (represented as “Known”) are taken from previous investigation (Jia et al., 2012; Voit and Almeida, 2004)

Kinetic Parameter	Parameter values comparison			
	Void and Almeida, 2004	Jia et al.	CRFIEKF	Status
γ_1	20	19.9999	20	Known
γ_2	8	7.9998	8	Known
γ_3	3	2.9998	3	Known
γ_4	5	4.9998	5	Known
γ_5	2	2.0002	2	Known
γ_6	6	5.9997	6	Known
f_{13}	0.8	0.8	0.65	Estimated
f_{21}	0.5	0.5	0.40	Estimated
f_{32}	0.75	0.75	0.85	Estimated
f_{43}	0.5	0.5	0.48	Estimated
f_{44}	0.2	0.2	0.23	Estimated
f_{51}	0.5	0.4999	0.38	Estimated
f_{64}	0.8	0.7999	0.09	Estimated

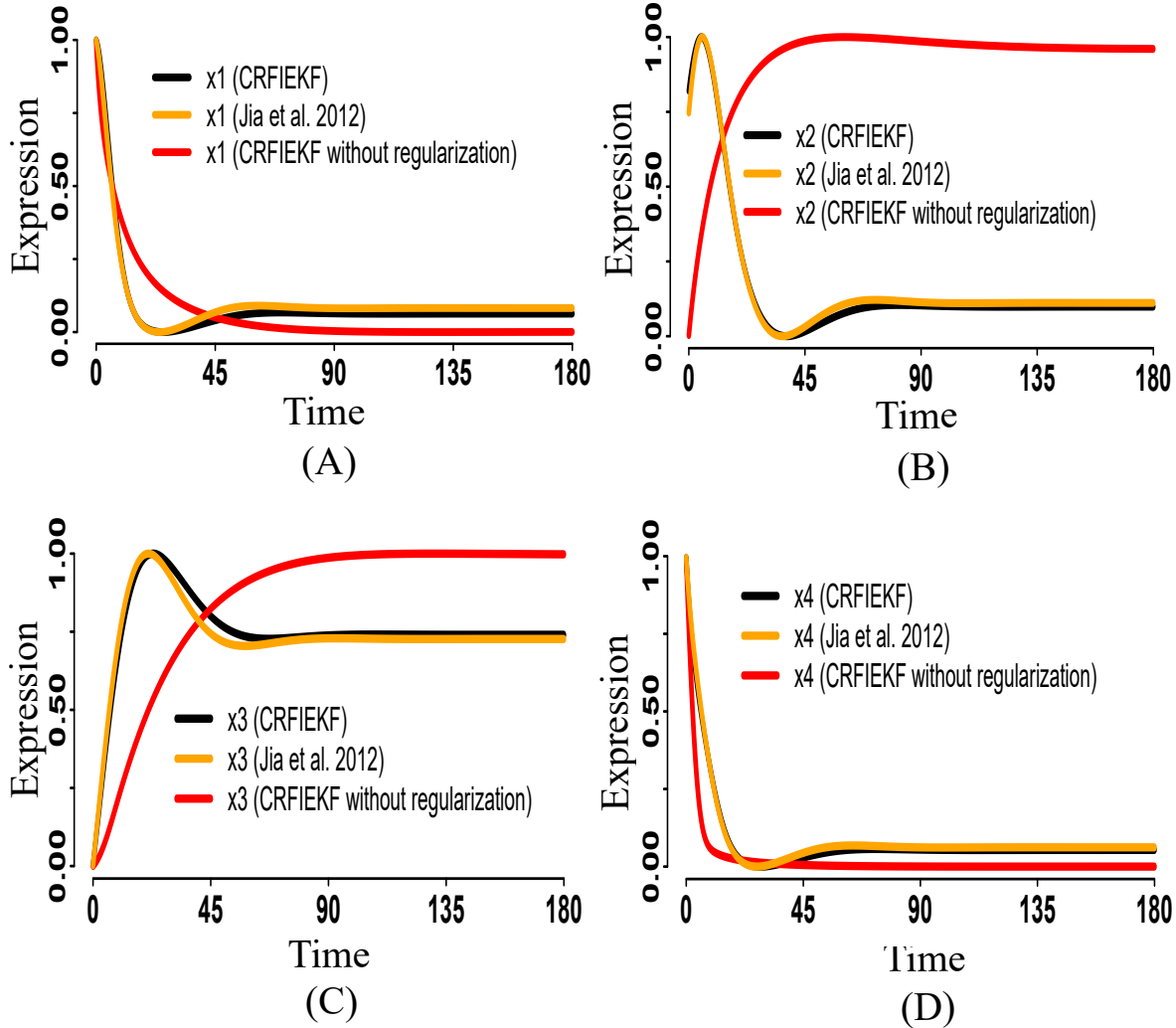


Figure 2. The figure illustrates the comparison of dynamics of x_1 , x_2 , x_3 , and x_4 of the generic branch pathway model using the parameter values estimated by CRFIEKF with Tikhonov regularization, CRFIEKF without any regularization and the actual parameter values given by Jia et al. (Jia et al., 2012). The different dynamics compared to actual ones because of the estimated parameters using CRFIEKF without any regularization indicated the effectiveness of the regularization technique.

Table 7. The table represents the sensitivity matrix of the generic branch pathway model. It represents the sensitivity of the output variables concerning changes in the values of the parameters. In MATLAB, we determined the rank of the matrix to be 13. This result indicates that the sensitivity matrix is full rank, suggesting that the model is identifiable based on the estimated parameter values.

0.40	0.99	0.00	0.54	1.07	0.08	0.31	0.03	0.11	0.00	0.11	0.04	0.03
1.05	0.22	1.34	1.43	2.83	0.23	0.81	0.09	0.02	0.72	0.30	0.10	0.07
1.92	1.27	0.00	2.62	5.20	1.33	1.49	0.17	0.14	0.00	0.55	0.59	0.13
0.08	0.21	0.00	0.12	0.23	0.22	0.42	0.01	0.02	0.00	0.02	0.10	0.04
11.47	19.69	36.43	70.10	135.24	21.52	38.64	0.94	2.39	18.52	14.45	10.10	3.47
28.14	83.42	568.40	42.93	82.61	19.88	23.64	2.48	15.55	75.70	8.82	9.34	2.13
24.32	3.18	100.64E2	29.46	56.91	3.77	16.24	221.87	0.37	0.50	6.10	1.66	1.46
10.44	22.03	9.50	5.40	56.46	0.76	5.38	0.92	2.69	2.09	6.17	0.27	0.48
5.74	12.25	0.23	6.93	13.37	13.00	3.10	2.56	1.47	0.12	1.43	6.20	4.39
7.61	11.44	36.26	65.44	126.22	29.19	43.79	1.28	1.40	18.43	13.49	10.33	3.94
9.53	20.35	11.84	16.63	32.10	3.04	9.19	0.80	2.57	3.17	3.42	1.44	0.82
17.56	36.38	1.18	20.80	40.31	9.79	11.54	1.59	4.55	0.48	4.36	4.97	2.89
1.26	12.99	6.62	1.55	3.05	28.27	0.87	0.11	1.54	3.27	0.33	5.49	0.08
18.42	48.39	5.45	21.81	42.30	18.39	10.98	1.67	5.99	2.79	4.57	10.50	2.84
4.77	11.12	3.86	33.59	86.05	12.62	24.50	0.37	1.46	10.92	9.32	6.07	2.23
11.29	27.88	62.38	84.02	161.72	28.96	46.25	1.02	3.28	21.90	17.28	13.52	4.16
8.40	17.90	1846.39	16.38	34.41	10.01	21.23	0.74	2.16	177.47	5.01	4.74	1.93

Table 8. The table represents the correlation coefficient of the parameter values of the generic branch pathway model (Jia et al., 2012). The rows and columns represent the kinetic parameters involved in the pathway. The correlation matrix having more than 60% absolute value < 0.5 signifies that the model is distinguishable based on estimated parameter values.

	f_{13}	f_{21}	f_{32}	f_{43}	f_{44}	f_{51}	f_{64}	g_1	g_2	g_3	g_4	g_5	g_6
f_{13}	1.00												
f_{21}	-0.71	1.00											
f_{32}	0.35	-0.48	1.00										
f_{43}	-0.25	-0.12	-0.60	1.00									
f_{44}	0.20	0.23	0.58	-0.94	1.00								
f_{51}	0.13	-0.50	0.26	0.39	-0.34	1.00							
f_{64}	-0.12	0.36	0.35	-0.79	0.68	-0.43	1.00						
g_1	-0.36	0.50	-1.00	0.59	-0.58	-0.27	-0.34	1.00					
g_2	0.40	-0.92	0.49	0.27	-0.37	0.61	-0.37	-0.50	1.00				
g_3	-0.33	0.64	-0.96	0.38	-0.33	-0.42	-0.19	0.96	-0.70	1.00			
g_4	-0.19	-0.24	-0.57	0.94	-1.00	0.35	-0.69	0.57	0.39	0.32	1.00		
g_5	0.66	-0.37	0.33	-0.56	0.44	-0.51	0.24	-0.34	0.10	-0.24	-0.44	1.00	
g_6	-0.09	-0.16	0.83	-0.45	0.50	0.33	0.33	-0.83	0.31	-0.80	-0.49	-0.12	1.00

3. Parameter estimation of Mammalian glycolysis pathway

Glycolysis, a metabolic pathway, plays a fundamental role in converting glucose into pyruvate through a series of biochemical reactions, releasing a substantial amount of energy in the form of ATP and NADH molecules (Nelson et al., 2008; Bolaños et al., 2010). Under normoxia conditions, most pyruvate molecules are utilized in the TCA cycle to initiate oxidative phosphorylation, resulting in lower lactate production than hypoxia. The interactions among the molecules involved in this pathway are illustrated in Supplementary Figure 3. We employed a modified version of the Michaelis-Menten equation (Paul et al., 2015) to construct the state-space model of the pathway. This formulation introduces unknown kinetic parameters, including catalytic rate constants, Michaelis rate constants, and feedback constants. Our study focused on 22 pathway reactions obtained from KEGG (Kanehisa and Goto, 2000). We presented in Supplementary Tables 9-11, which detail the biochemical reactions, equations of reaction fluxes, and the stoichiometric matrix.

The state-space model encompasses a total of 47 kinetic parameters. Unlike previous methods, our approach relies on something other than prior knowledge of time-course experimental measurements. Instead, we generated an approximated measurement using a fuzzy inference system (FIS) based on known imprecise relationships among 15 metabolites and enzymes, as outlined in Supplementary Tables 12-16. The universe of discourse for the metabolites and enzymes was assumed to be within the range [0, 1]. Subsequently, we estimated the parameter values while varying the regularization techniques (Tikhonov, L1, and a hybrid of both), membership functions (Gaussian, Generalized Bell, Triangular, and Trapezoidal) of the FIS blocks, and the number of approximated measurements. The dynamics of eight metabolites (Glucose 6 phosphate, Fructose 6 phosphate, Fructose 1,6 bisphosphate, Dihydroxyacetone phosphate, 3 phosphoglycerate, Phosphoenol pyruvate, Pyruvate, and Lactate) in hypoxia-induced mammalian erythrocytes were observed using these estimated parameter values. The perturbed activities of these metabolites are presented in Supplementary Figures 4-5, and the corresponding MSEs are summarized in Supplementary Tables 17-18. Interestingly, we found that the dynamics of the metabolites did not significantly differ across various settings, indicating that any regularization technique and membership function can be effectively employed in the estimation process. For our methodology, we chose Tikhonov regularization and Gaussian membership functions.

Additionally, we estimated the same set of parameter values using the approach of Lillacci et al. (Lillacci and Khammash, 2010), utilizing capillary electrophoresis mass spectrometry (CE-MS) measured concentration values (Kinoshita et al., 2007) (normalized in [0, 1]) associated with hypoxia-induced human erythrocytes as the measurement signal. Subsequently, we assessed the perturbed activities of eight metabolites in the glycolysis pathway of hypoxia-induced human erythrocytes, individually using the parameter values estimated by our proposed method and the previous investigation (Lillacci and Khammash, 2010). It should be noted that the activities of several related enzymes need to be modified, as evidenced by Kinoshita et al. (Kinoshita et al., 2007). We then compared the resulting behavior of these eight metabolites with the findings from the previous *in silico/in vitro* investigation (Kinoshita et al., 2007). Remarkably, the MSEs of the dynamics of these metabolites using our proposed method, Lillacci et al. (Lillacci and Khammash, 2010), and Kinoshita et al. (Kinoshita et al., 2007) were found to be significantly close ($p < 0.001$), highlighting the effectiveness of our approach. Supplementary Figures 7-8 depict the perturbed activity of these metabolites.

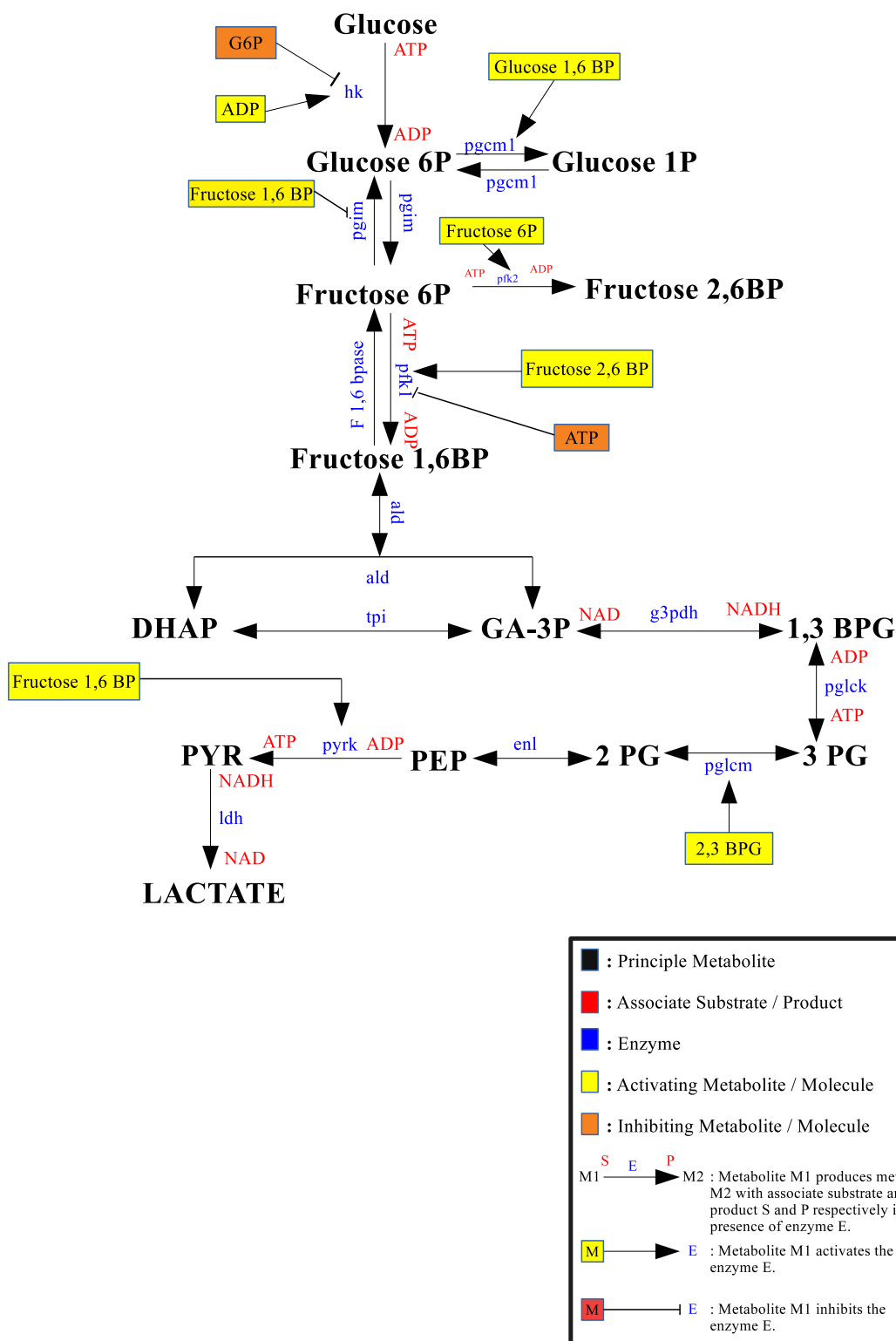


Figure 3. This figure depicts the reduced glycolysis pathway under consideration. We consider 22 reactions of the pathway collected from KEGG (Kanehisa and Goto, 2000)

Table 9. Reaction list contains 22 reactions from the KEGG database for the mammalian glycolysis pathway under consideration.

-
1. Glucose + ATP \Rightarrow Glucose 6-phosphate + ADP
 2. Glucose 6-phosphate \Rightarrow Glucose
 3. Glucose 6-phosphate \Rightarrow Fructose 6-phosphate
 4. Fructose 6-phosphate \Rightarrow Glucose 6-phosphate
 5. Fructose 6-phosphate + ATP \Rightarrow Fructose 1,6-bisphosphate + ADP
 6. Fructose 1,6-bisphosphate \Rightarrow Fructose 6-phosphate
 7. Fructose 6-phosphate + ATP \Rightarrow Fructose 2,6-bisphosphate + ADP
 8. Fructose 2,6-bisphosphate \Rightarrow Fructose 6-phosphate
 9. Fructose 1,6BP \Rightarrow Dihydroxyacetone phosphate + Glyceraldehyde 3-phosphate
 10. Dihydroxyacetone phosphate + Glyceraldehyde 3-phosphate \Rightarrow Fructose-1,6BP
 11. Dihydroxyacetone phosphate \Rightarrow Glyceraldehyde 3-phosphate
 12. Glyceraldehyde 3-phosphate \Rightarrow Dihydroxyacetone phosphate
 13. Glyceraldehyde 3-phosphate + NAD \Rightarrow 1,3-Bisphosphoglycerate + NADH
 14. 1,3-Bisphosphoglycerate + NADH \Rightarrow Glyceraldehyde 3-phosphate + NAD
 15. 1,3-Bisphosphoglycerate + ADP \Rightarrow 3-Phosphoglycerate + ATP
 16. 3-Phosphoglycerate \Rightarrow 1,3-Bisphosphoglycerate
 17. 3-Phosphoglycerate \Rightarrow 2-Phosphoglycerate
 18. 2-Phosphoglycerate \Rightarrow 3-Phosphoglycerate
 19. 2-Phosphoglycerate \Rightarrow Phosphoenolpyruvate
 20. Phosphoenolpyruvate \Rightarrow 2-Phosphoglycerate
 21. Phosphoenolpyruvate + ADP \Rightarrow Pyruvate + ATP
 22. Pyruvate + NADH \Rightarrow Lactate + NAD
-

Table 10. Reaction equations contains the equations of reaction fluxes associated with 22 reactions from the KEGG database for the mammalian glycolysis pathway under consideration.

1.	$v_1 = \frac{((K_{hexokinase} \cdot [hexokinase] \cdot [glucose] \cdot [ATP]) \cdot (1 + F_1 \cdot [ADP]))}{(Km_1 + [glucose] \cdot [ATP]) \cdot (1 + F_2 \cdot [glucose6P])}$
2.	$v_2 = \frac{(K_{glucose6Pase} \cdot [glucose6Pase] \cdot [glucose6P] \cdot (1 + F_3 \cdot [glucose6P]))}{(km_2 + [glucose6P])}$
3.	$v_3 = \frac{(k_{phosphoglucoisomerase} \cdot [phosphoglucoisomerase] \cdot [glucose6P])}{((Km_3 + [glucose6P]) \cdot (1 + F_4 \cdot [fructose1,6BP]))}$
4.	$v_4 = \frac{(K_{phosphoglucoisomerase} \cdot [phosphoglucoisomerase] \cdot [fructose6P])}{((Km_4 + [fructose6P]) \cdot (1 + F_5 \cdot [fructose1,6BP]))}$
5.	$v_5 = \frac{((K_{phosphofructokinase1} \cdot [phosphofructokinase1] \cdot [fructose6P] \cdot [ATP]) \cdot (1 + F_6 \cdot [f_26BP]))}{((Km_5 + [fructose6P] \cdot [ATP]) \cdot (1 + F_7 \cdot [ATP]))}$
6.	$v_6 = \frac{(K_{fructose1,6Bpase} \cdot [fructose1,6Bpase] \cdot [fructose1,6BP])}{(Km_6 + [fructose1,6BP]) \cdot (1 + F_8 \cdot [fructose2,6BP])}$
7.	$v_7 = \frac{((K_{phosphofructokinase2} \cdot [phosphofructokinase2] \cdot [fructose6P] \cdot [ATP]) \cdot (1 + F_9 \cdot [fructose6P]))}{((Km_7 + [fructose6P] \cdot [ATP]))}$
8.	$v_8 = \frac{(K_{fructose2,6Bpase} \cdot [fructose2,6Bpase] \cdot [fructose2,6BP])}{(Km_8 + [fructose2,6BP]) \cdot (1 + F_{10} \cdot [fructose6P])}$
9.	$v_9 = \frac{(K_{aldolase} \cdot [aldolase] \cdot [fructose1,6BP])}{(Km_9 + [fructose1,6BP])}$
10.	$v_{10} = \frac{(K_{aldolase} \cdot [aldolase] \cdot [dihydroxyacetonephosphate] \cdot [glyceraldehyde3P])}{(Km_{10} + [dihydroxyacetonephosphate] \cdot [glyceraldehyde3P])}$
11.	$v_{11} = \frac{(K_{triosephosphateisomerase} \cdot [triosephosphateisomerase] \cdot [dihydroxyacetonephosphate])}{(Km_{11} + [dihydroxyacetonephosphate])}$
12.	$v_{12} = \frac{(K_{triosephosphateisomerase} \cdot [triosephosphateisomerase] \cdot [glyceraldehyde3P])}{(Km_{12} + [glyceraldehyde3P])}$
13.	$v_{13} = \frac{(K_{Glyceraldehyde3Pdehydrogenase} \cdot [Glyceraldehyde3Pdehydrogenase] \cdot [glyceraldehyde3P] \cdot [NAD])}{(Km_{13} + [glyceraldehyde3P] \cdot [NAD])}$
14.	$v_{14} = \frac{(K_{Glyceraldehyde3Pdehydrogenase} \cdot [Glyceraldehyde3Pdehydrogenase] \cdot [1,3bisphosphoglycerate] \cdot [NADH])}{(Km_{14} + [1,3bisphosphoglycerate] \cdot [NADH])}$
15.	$v_{15} = \frac{(K_{Phosphogluokinase} \cdot [Phosphoglucoisomerase] \cdot [1,3bisphosphoglycerate] \cdot [ADP])}{(Km_{15} + [1,3bisphosphoglycerate] \cdot [ADP])}$
16.	$v_{16} = \frac{(K_{Phosphogluokinase} \cdot [Phosphoglucoisomerase] \cdot [3phosphoglycerate])}{(Km_{16} + [3phosphoglycerate])}$
17.	$v_{17} = \frac{((K_{phosphoglucomutase} \cdot [phosphoglucomutase] \cdot [3phosphoglycerate]) \cdot (1 + F_{24} \cdot [2,3bisphosphoglycerate]))}{(Km_{17} + [3phosphoglycerate])}$
18.	$v_{18} = \frac{((K_{phosphoglucomutase} \cdot [phosphoglucomutase] \cdot [2phosphoglycerate]) \cdot (1 + F_{25} \cdot [2,3bisphosphoglycerate]))}{(Km_{18} + [2phosphoglycerate])}$
19.	$v_{19} = \frac{(K_{enolase} \cdot [enolase] \cdot [2phosphoglycerate])}{(Km_{19} + [2phosphoglycerate])}$
20.	$v_{20} = \frac{(K_{enolase} \cdot [enolase] \cdot [phosphoenolpyruvate])}{(Km_{20} + [phosphoenolpyruvate])}$
21.	$v_{21} = \frac{((K_{pyruvatekinase} \cdot [pyruvatekinase] \cdot [phosphoenolpyruvate] \cdot [ADP]) \cdot (1 + F_{11} \cdot [fructose1,6BP]))}{((Km_{21} + [phosphoenolpyruvate] \cdot [ADP]) \cdot (1 + F_{12} \cdot [ATP]))}$
22.	$v_{22} = \frac{(K_{lactatedehydrogenase} \cdot [lactatedehydrogenase] \cdot [pyruvate] \cdot [NADH])}{(Km_{22} + [pyruvate] \cdot [NADH])}$

Table 11. It contains the stoichiometric matrix associated with 22 reactions from the KEGG database for the mammalian glycolysis pathway under consideration. The rows represent the metabolites involved in the pathway, whereas the columns represent fluxes associated with each reaction.

	v1	v2	v3	v4	v5	v6	v7	v8	v9	v10	v11	v12	v13	v14	v15	v16	v17	v18	v19	v20	v21	v22
Glucose 6 phosphate	1	-1	-1	1	0	0	0	0	0	0	0	0	0	0	0	0	0	0	0	0	0	
Glucose	-1	1	0	0	0	0	0	0	0	0	0	0	0	0	0	0	0	0	0	0	0	
Fructose 6 phosphate	0	0	1	-1	-1	1	-1	1	0	0	0	0	0	0	0	0	0	0	0	0	0	
Fructose 1,6 Bisphosphate	0	0	0	0	1	-1	0	0	-1	1	0	0	0	0	0	0	0	0	0	0	0	
Fructose 2,6 Bisphosphate	0	0	0	0	0	0	1	-1	0	0	0	0	0	0	0	0	0	0	0	0	0	
Dihydroxyacetone phosphate	0	0	0	0	0	0	0	0	1	-1	-1	1	0	0	0	0	0	0	0	0	0	
Glyceraldehyde 3-phosphate	0	0	0	0	0	0	0	0	0	1	-1	-1	1	0	0	0	0	0	0	0	0	
1,3-Bisphosphoglycerate	0	0	0	0	0	0	0	0	0	0	0	0	1	-1	1	0	0	0	0	0	0	
3 phosphoglycerate	0	0	0	0	0	0	0	0	0	0	0	0	0	0	1	-1	1	0	0	0	0	
2 phosphoglycerate	0	0	0	0	0	0	0	0	0	0	0	0	0	0	0	1	-1	1	0	0	0	
Phosphoenol pyruvate	0	0	0	0	0	0	0	0	0	0	0	0	0	0	0	0	0	1	-1	0	0	
Pyruvate	0	0	0	0	0	0	0	0	0	0	0	0	0	0	0	0	0	0	0	1	-1	
Lactate	0	0	0	0	0	0	0	0	0	0	0	0	0	0	0	0	0	0	0	0	0	
ATP	-1	0	0	0	-1	0	-1	0	0	0	0	0	0	0	0	0	0	0	0	1	0	
ADP	1	0	0	0	1	0	1	0	0	0	0	0	0	0	-1	0	0	0	0	-1	0	
NADH	0	0	0	0	0	0	0	0	0	0	0	0	1	-1	0	0	0	0	0	-1	0	
NAD	0	0	0	0	0	0	0	0	0	0	0	0	-1	1	0	0	0	0	0	0	1	

Table 12. This table shows the names of 15 fuzzy molecules of the FIS used to estimate the parameter of the glycolysis pathway.

	Input metabolite list	Output metabolite list
FIS 1	Glucose, Pyruvate kinase	Pyruvate
FIS 2	Hexokinase, ATP, Glucose	Glucose 6 Phosphate, ADP
FIS 3	Glyceraldehyde 3P, Glyceraldehyde 3P Dehydrogenase , NAD	1,3 bisphosphoglycerate, NADH
FIS 4	Fructose 6 Phosphate, Phosphofructokinase 1	Fructose 1,6 bisphosphate

Table 13. IF–THEN rule base for FIS to capture fuzzy relationship between glucose & pyruvate kinase & Pyruvate

IF (glucose & pyruvate kinase)		Then pyruvate
Glucose	pyruvate kinase	Pyruvate
LOW	LOW	LOW
LOW	MEDIUM	LOW
LOW	HIGH	MEDIUM
MEDIUM	LOW	LOW
MEDIUM	MEDIUM	MEDIUM
MEDIUM	HIGH	MEDIUM
HIGH	LOW	LOW
HIGH	MEDIUM	MEDIUM
HIGH	HIGH	HIGH

Table 14. IF–THEN rule base for FIS to capture fuzzy relationship between hexokinase & ATP & glucose and Glucose6 Phosphate & ADP

IF (hexokinase & ATP & glucose)			Then (Glucose 6 Phosphate & ADP)	
Hexokinase	ATP	Glucose	Glucose 6 Phosphate	ADP
LOW	LOW	LOW	LOW	HIGH
LOW	LOW	MEDIUM	LOW	HIGH
LOW	LOW	HIGH	MEDIUM	HIGH
LOW	MEDIUM	LOW	LOW	MEDIUM
LOW	MEDIUM	MEDIUM	MEDIUM	MEDIUM
LOW	MEDIUM	HIGH	MEDIUM	MEDIUM
LOW	HIGH	LOW	LOW	LOW
LOW	HIGH	MEDIUM	MEDIUM	LOW
LOW	HIGH	HIGH	MEDIUM	LOW
MEDIUM	LOW	LOW	LOW	HIGH
MEDIUM	LOW	MEDIUM	MEDIUM	HIGH
MEDIUM	LOW	HIGH	MEDIUM	HIGH
MEDIUM	MEDIUM	LOW	LOW	MEDIUM
MEDIUM	MEDIUM	MEDIUM	MEDIUM	MEDIUM
MEDIUM	MEDIUM	HIGH	MEDIUM	MEDIUM
MEDIUM	HIGH	LOW	LOW	LOW
MEDIUM	HIGH	MEDIUM	MEDIUM	LOW
MEDIUM	HIGH	HIGH	MEDIUM	LOW
HIGH	LOW	LOW	LOW	HIGH
HIGH	LOW	MEDIUM	MEDIUM	HIGH
HIGH	LOW	HIGH	MEDIUM	HIGH
HIGH	MEDIUM	LOW	LOW	MEDIUM
HIGH	MEDIUM	MEDIUM	MEDIUM	MEDIUM
HIGH	MEDIUM	HIGH	MEDIUM	MEDIUM
HIGH	HIGH	LOW	LOW	LOW
HIGH	HIGH	MEDIUM	MEDIUM	LOW
HIGH	HIGH	HIGH	HIGH	LOW

Table 15. IF–THEN rule base for FIS to capture fuzzy relationship between glyceraldehyde 3P & glyceraldehyde 3P deh & NAD and 1,3-BPG & NADH. Here, glyclrdh 3P, glyclrdh 3P deh, 1,3-BPG stands for glyceraldehyde 3 phosphate, glyceraldehyde 3 phosphate dehydrogenase, and 1,3 Biphosphoglycerate respectively.

IF glyclrdh 3P & glyclrdh 3P deh & NAD			Then 1,3-BPG & NADH	
glyclrdh 3P	glyclrdh 3P deh	NAD	1,3-BPG	NADH
LOW	LOW	LOW	LOW	LOW
LOW	LOW	MEDIUM	LOW	MEDIUM
LOW	LOW	HIGH	LOW	MEDIUM
LOW	MEDIUM	LOW	LOW	LOW
LOW	MEDIUM	MEDIUM	LOW	MEDIUM
LOW	MEDIUM	HIGH	MEDIUM	MEDIUM
LOW	HIGH	LOW	LOW	LOW
LOW	HIGH	MEDIUM	LOW	MEDIUM
LOW	HIGH	HIGH	LOW	MEDIUM
MEDIUM	LOW	LOW	LOW	LOW
MEDIUM	LOW	MEDIUM	LOW	MEDIUM
MEDIUM	LOW	HIGH	MEDIUM	MEDIUM
MEDIUM	MEDIUM	LOW	MEDIUM	MEDIUM
MEDIUM	MEDIUM	MEDIUM	MEDIUM	MEDIUM
MEDIUM	MEDIUM	HIGH	MEDIUM	HIGH
MEDIUM	HIGH	LOW	MEDIUM	LOW
MEDIUM	HIGH	MEDIUM	MEDIUM	MEDIUM
MEDIUM	HIGH	HIGH	MEDIUM	HIGH
HIGH	LOW	LOW	LOW	LOW
HIGH	LOW	MEDIUM	LOW	MEDIUM
HIGH	LOW	HIGH	LOW	MEDIUM
HIGH	MEDIUM	LOW	MEDIUM	LOW
HIGH	MEDIUM	MEDIUM	MEDIUM	MEDIUM
HIGH	MEDIUM	HIGH	MEDIUM	HIGH
HIGH	HIGH	LOW	HIGH	LOW
HIGH	HIGH	MEDIUM	HIGH	MEDIUM
HIGH	HIGH	HIGH	HIGH	HIGH

Table 16. IF – THEN rule base for FIS to capture fuzzy relationship between Fructose 6P & Pfk1 & ATP and Fructose 1,6BP. Here, pfk1 stands for phosphofructokinase 1.

IF Fructose 6P & Pfk1 & ATP			Then Fructose 1,6BP
Fructose 6P	Pfk1	ATP	Fructose 1,6BP
LOW	LOW	LOW	LOW
LOW	LOW	MEDIUM	LOW
LOW	LOW	HIGH	LOW
LOW	MEDIUM	LOW	LOW
LOW	MEDIUM	MEDIUM	LOW
LOW	MEDIUM	HIGH	LOW
LOW	HIGH	LOW	LOW
LOW	HIGH	MEDIUM	LOW
LOW	HIGH	HIGH	LOW
MEDIUM	LOW	LOW	LOW
MEDIUM	LOW	MEDIUM	LOW
MEDIUM	LOW	HIGH	LOW
MEDIUM	MEDIUM	LOW	MEDIUM
MEDIUM	MEDIUM	MEDIUM	MEDIUM
MEDIUM	MEDIUM	HIGH	MEDIUM
MEDIUM	HIGH	LOW	LOW
MEDIUM	HIGH	MEDIUM	MEDIUM
MEDIUM	HIGH	HIGH	MEDIUM
HIGH	LOW	LOW	MEDIUM
HIGH	LOW	MEDIUM	MEDIUM
HIGH	LOW	HIGH	MEDIUM
HIGH	MEDIUM	LOW	MEDIUM
HIGH	MEDIUM	MEDIUM	MEDIUM
HIGH	MEDIUM	HIGH	HIGH
HIGH	HIGH	LOW	MEDIUM
HIGH	HIGH	MEDIUM	HIGH
HIGH	HIGH	HIGH	HIGH

Table 17. This table demonstrates the MSE of dynamics of eight metabolites of hypoxia-induced human erythrocytes in Kinoshita et al.(Kinoshita et al., 2007) and proposed technique using the parameter values considering Tikhonov regularization, L1 regularization and a hybrid of them during the parameter estimation process.

Metabolite	MSE comparison		
	Kinoshita et al.(Kinoshita et al., 2007) vs CRFIEKF (Tokhonov regularized)	Kinoshita et al.(Kinoshita et al., 2007) vs CRFIEKF (L1 regularized)	Kinoshita et al.(Kinoshita et al., 2007) vs CRFIEKF (combined regularized)
Glucose 6 phosphate	0.0150	0.0163	0.0213
Fructose 6 phosphate	0.0054	0.0056	0.0060
Fructose 1,6 bisphosphate	0.1506	0.0744	0.0113
Dihydroxyacetone phosphate	0.0488	0.0972	0.1721
3 Phosphoglycerate	0.1325	0.0148	0.2629
Phosphoenol pyruvate	0.4366	0.5865	0.6222
Pyruvate	0.0747	0.1184	0.2167
Lactate	0.0148	0.0292	0.0835

Comparison of dynamics of 8 metabolites using proposed method considering Tikhonov, L1 and the combination of both regularization respectively and simulation result by Kinoshita et al.

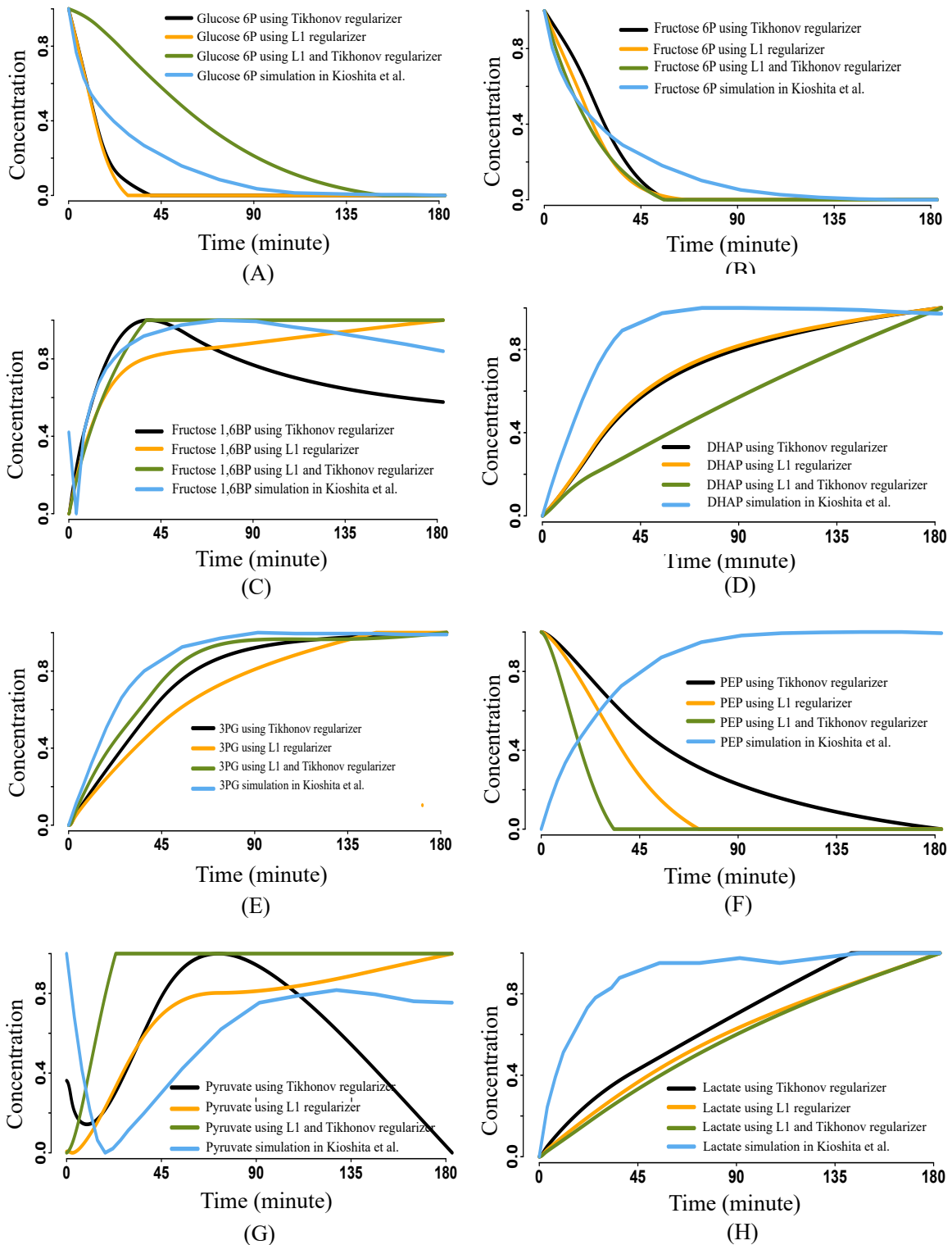


Figure 4. This figure demonstrates the dynamics of 8 metabolites during hypoxia using the parameter values estimated by the proposed method. Here, we separately estimate the parameter values incorporating L1 regularization, Tikhonov regularization, and a combined L1 followed by Tikhonov regularization. Afterward, we separately capture the perturbed activities of eight metabolites of the glycolysis pathway of hypoxia-induced human erythrocytes. We observe that L1 and the Tikhonov regularized technique have similar influence on the dynamics of hypoxia-induced human erythrocytes(Kinoshita et al., 2007). However, incorporating the combination of L1 followed by the Tikhonov regularization slightly deviates the trajectories. The result confirms the effectiveness of employing Tikhonov regularization in the proposed technique.

Comparison of dynamics of 8 metabolites using the proposed method considering Gaussian, Generalized bell, Triangular, and Trapezoidal membership functions, respectively, and simulation results by Kinoshita et al.

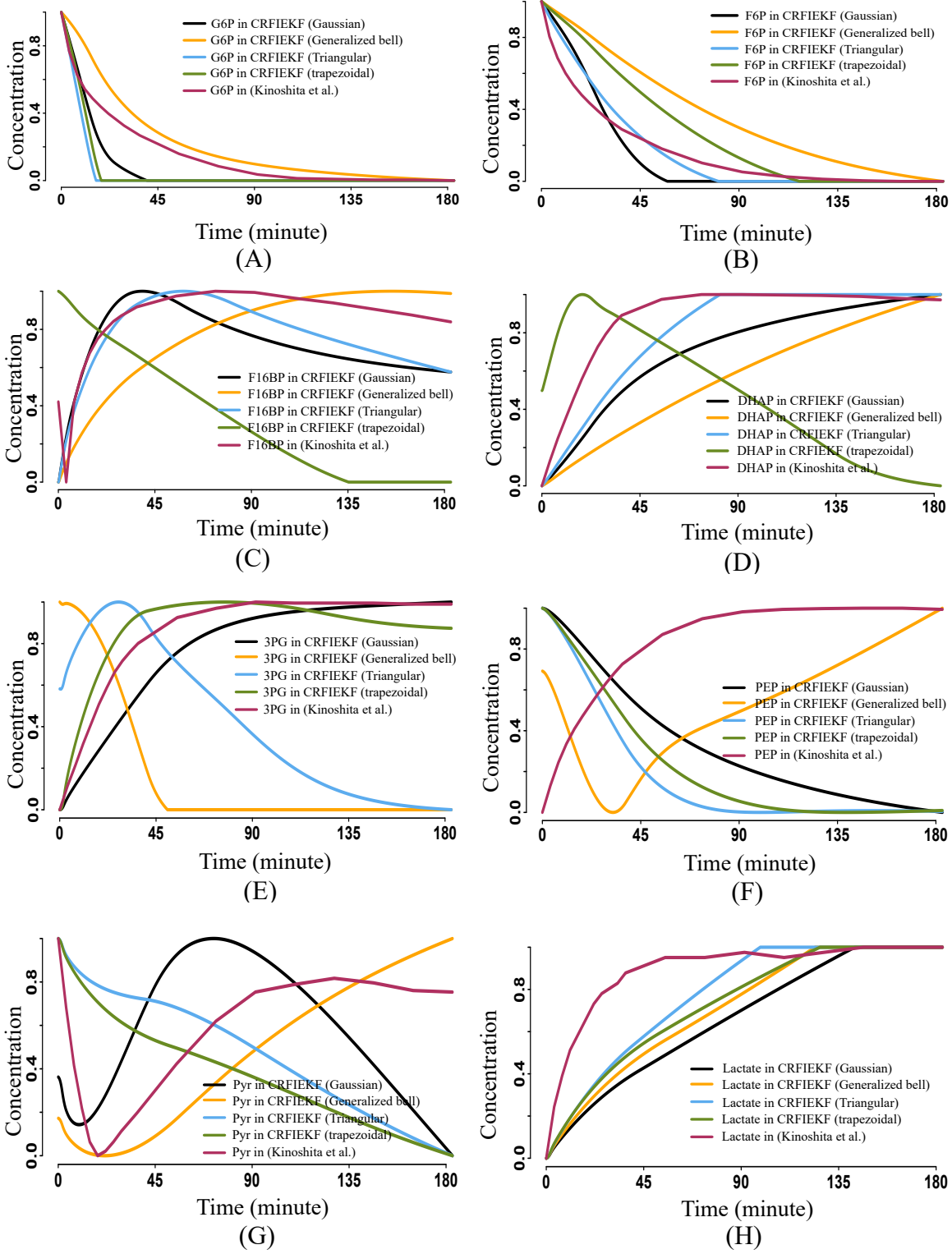


Figure 5. This figure demonstrates the dynamics of 8 metabolites during hypoxia using the parameter values estimated by the proposed method. Here, we separately estimate the parameter values considering Gaussian, Generalized bell, Triangular, and Trapezoidal membership functions in the FIS. Afterward, we separately capture the perturbed activities of eight metabolites of the glycolysis pathway of hypoxia-induced human erythrocytes. We obtain the most similar dynamics as Kinoshita et al. (Kinoshita et al., 2007), with the help of parameter values estimated by CRFIEKF having Gaussian membership function in the FIS. The result confirms the effectiveness of using the Gaussian membership function in the investigation.

Table 18. This table demonstrates the MSE of dynamics of eight metabolites of hypoxia-induced human erythrocytes in Kinoshita et al.(Kinoshita et al., 2007) and proposed technique using the parameter values considering membership function (MF) of the FIS block as Gaussian, Generalized Bell, Triangular and Trapezoidal during the parameter estimation process.

Metabolite	MSE comparison			
	Kinoshita et al.(Kinoshita et al., 2007) vs CRFIEKF (Gaussian MF)	Kinoshita et al.(Kinoshita et al., 2007) vs CRFIEKF (Generalized Bell MF)	Kinoshita et al.(Kinoshita et al., 2007) vs CRFIEKF (Triangular MF)	Kinoshita et al.(Kinoshita et al., 2007) vs CRFIEKF (Trapezoidal MF)
Glucose 6 phosphate	0.0150	0.0180	0.0218	0.0193
Fructose 6 phosphate	0.0054	0.0529	0.0051	0.0223
Fructose 1,6 bisphosphate	0.1506	0.1094	0.1106	0.5015
Dihydroxyacetone phosphate	0.0488	0.1843	0.0092	0.2583
3 Phosphoglycerate	0.1325	0.6305	0.4312	0.1806
Phosphoenol pyruvate	0.4366	0.1007	0.3292	0.2527
Pyruvate	0.0747	0.0580	0.1158	0.1135
Lactate	0.0148	0.0115	0.0084	0.0098

Table 19. This table demonstrates the MSE of dynamics of eight metabolites of hypoxia-induced human erythrocytes in Kinoshita et al.(Kinoshita et al., 2007) and proposed technique using the parameter values considering 4, 5, 6 approximated measurement based on the known imprecise relationship among the molecules of the pathway during the parameter estimation process.

Metabolite	MSE comparison		
	Kinoshita et al.(Kinoshita et al., 2007) vs CRFIEKF (6 approximated measurement)	Kinoshita et al.(Kinoshita et al., 2007) vs CRFIEKF (5 approximated measurement)	Kinoshita et al.(Kinoshita et al., 2007) vs CRFIEKF (4 approximated measurement)
Glucose 6 phosphate	0.0150	0.0154	0.0154
Fructose 6 phosphate	0.0054	0.0386	0.0058
Fructose 1,6 bisphosphate	0.1506	0.0278	0.1051
Dihydroxyacetone phosphate	0.0488	0.1428	0.0458
3 Phosphoglycerate	0.1325	0.2254	0.4272
Phosphoenol pyruvate	0.4366	0.6138	0.3027
Pyruvate	0.0747	0.1552	0.0666
Lactate	0.0148	0.0084	0.0479

Table 20. (A) We separately estimate the parameter values by altering the regularization technique in the proposed method. Afterward, using the parameter values for each of three regularization techniques, such as Tikhonov, L1, and a hybrid of both, we evaluate the MSEs of the dynamics of eight metabolites of hypoxia-induced human erythrocytes based on the simulation result and CE-MS measurement (normalized in [0, 1])(Kinoshita et al., 2007). In this way, we develop two cases, each comprising three sets of MSEs of eight metabolites corresponding to three regularization techniques. On performing the ANOVA test among the three sets of MSEs in both cases, we observed the F-statistic value < F-critical value. Such a result shows that regularization techniques have no significantly different influence on parameter estimation techniques. In (B), we obtain the MSE of eight metabolites similar to that mentioned in (A) using parameter values estimated by altering Gaussian, Generalized bell, Triangular, and Trapezoidal membership functions distinctly. Unlike (A), each case comprises four sets of MSEs of eight metabolites corresponding to four membership functions. We further notice the F-statistic value < F-critical value in both cases. Such a result indicates that the proposed technique does not generate significantly different results when altering membership functions. Finally, in (C), similar to the cases above, altering the number of approximated observations (four/five/six), each of the two cases comprises three sets of MSEs corresponding to the number of approximated observations. In this case, also we observe the F-statistic value < F-critical value. Such a result supports the claim of robustness of the estimation technique. Here, all the claims have been considered at a 95% significance level. The column name “F-stat” and “F-crit” represent “F-statistics” and “F-critical” respectively.

Type	ANOVA test result			
	MSE based on	F-stat	P-value	F-crit
A. Regularization comparison	<i>in silico</i> simulation	0.2973	0.7459	3.4668
	CE-MS measurement	0.8195	0.4543	3.4668
B. Membership function comparison	<i>in silico</i> simulation	0.1772	0.911	2.9467
	CE-MS measurement	0.4161	0.7428	2.9467
C. Number of measurement comparison	<i>in silico</i> simulation	0.1365	0.8732	3.4668
	CE-MS measurement	1.0906	0.3543	3.4668

Comparison of dynamics of 8 metabolites using proposed method
considering 6, 5 and 4 approximate observation respectively
and simulation result by Kinoshita et al.

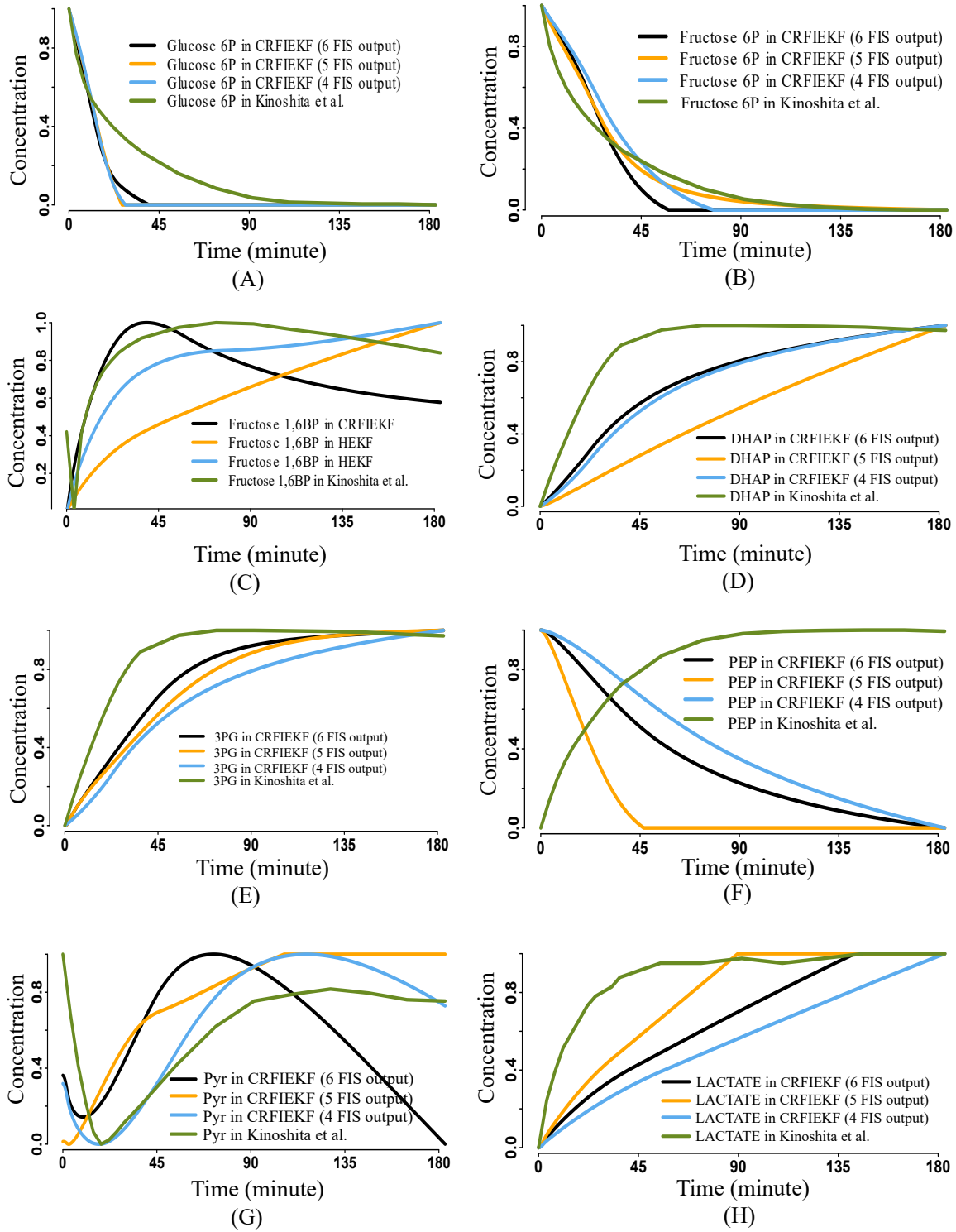


Figure 6. This figure demonstrates the dynamics of 8 metabolites during hypoxia using the parameter values estimated by the proposed method. Here, we separately estimate the parameter values assuming 6, 5, and 4 approximate observations from the FIS. Afterward, we separately capture the perturbed activities of eight metabolites of the glycolysis pathway of hypoxia-induced human erythrocytes. Despite altering the number of observations, the dynamics show almost similar behavior (The MSE for all the metabolites are not significantly different at $p < 0.001$.) as the simulation result by Kinoshita et al. (Kinoshita et al., 2007). This result validates the robustness of the proposed methodology.

Table 21. This table depicts the initial value and estimated value of 47 parameters in the glycolysis pathway.

Constant type	Parameter name	Initial value	Estimated value
Michaelis menten constant	km_1	0.052076	0.713900953
	km_2	0.4479	0.295157569
	km_3	0.052373	0.999467309
	km_4	0.4289	0.559038695
	km_5	0.054248	0.881503044
	km_6	0.4654	0.150000318
	km_7	0.053261	0.857460471
	km_8	0.07412	0.101167381
	km_9	0.1	0.426330857
	km_{10}	0.4415	0.632187475
	km_{11}	0.09692	0.9999
	km_{12}	0.7	0.815084321
	km_{13}	0.051036	0.968071306
	km_{14}	0.4729	0.445439606
	km_{15}	0.2	0.122681749
	km_{16}	0.4658	0.660009019
	km_{17}	0.053377	0.770427701
	km_{18}	0.3951	0.100012031
	km_{19}	0.073413	0.599673996
	km_{20}	0.42947	0.71799882
	km_{21}	0.13745	0.957762128
	km_{22}	0.7	0.233415694
Kinatic rate constant	$K_{hexokinase}$	0.02	0.673164996
	$K_{glucose6Pase}$	0.05	0.928702688
	$K_{phosphoglucoisomerase}$	0.0812	0.97646051
	$K_{phosphofructokinase1}$	0.09	0.968551348
	$K_{phosphofructokinase2}$	0.09	0.749009801
	$K_{aldolase}$	0.0826	0.485551038
	$K_{triosephosphateisomerase}$	0.0899	0.990298839
	$K_{Glyceraldehyde3Pdehydrogenase}$	0.01	0.672711844
	$K_{Phosphoglucokinase}$	0.0532	0.569340445
	$K_{phosphoglucomutase}$	0.06	0.299129342
	$K_{enolase}$	0.0727	0.100009938
	$K_{pyruvatekinase}$	0.2	0.833384647
	$K_{lactatedehydrogenase}$	0.01	0.669398944
	F_1	0.5	0.847604148
Feedback constant	F_2	0.5	0.853760185
	F_3	0.5	0.814920604
	F_4	0.5	0.206016679
	F_5	0.5	0.89288036
	F_6	0.5	0.168305091
	F_7	0.5	0.966223314
	F_8	0.5	0.50000004
	F_9	0.5	0.169828564
	F_{10}	0.5	0.50000004
	F_{11}	0.5	0.904357963
	F_{12}	0.5	0.466043176

Comparison of dynamics of 4 metabolites using proposed method, HEKF (Lillacci et al.(2010)) and simulation result by Kinoshita et al. (2007).

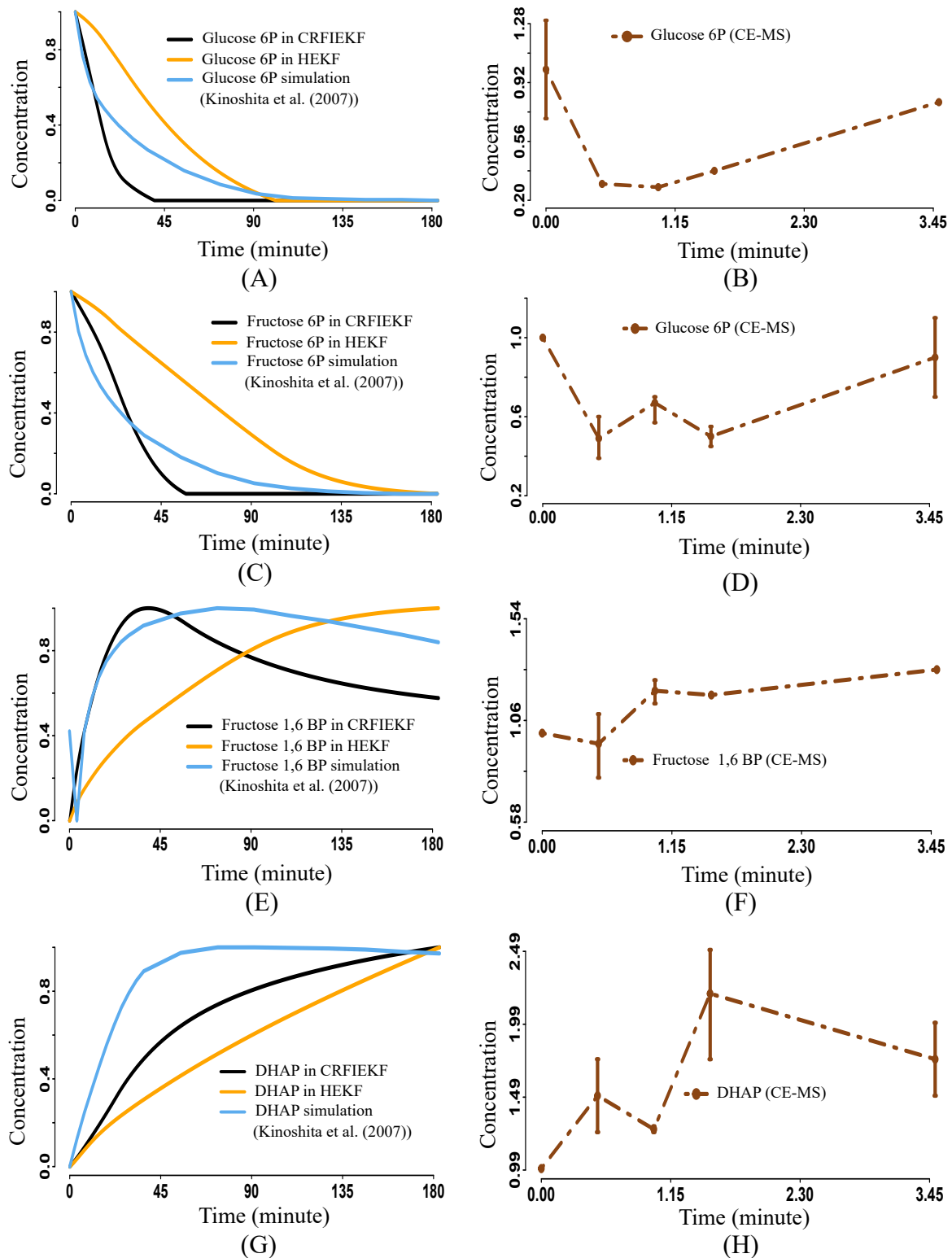


Figure 7. Validation of the proposed model during hypoxia through CE-MS measurement and simulation in human erythrocytes (Kinoshita et al. (Kinoshita et al., 2007)).

Comparison of dynamics of 4 metabolites using proposed method, HEKF (Lillacci et al.(2010)) and simulation result by Kinoshita et al. (2007).

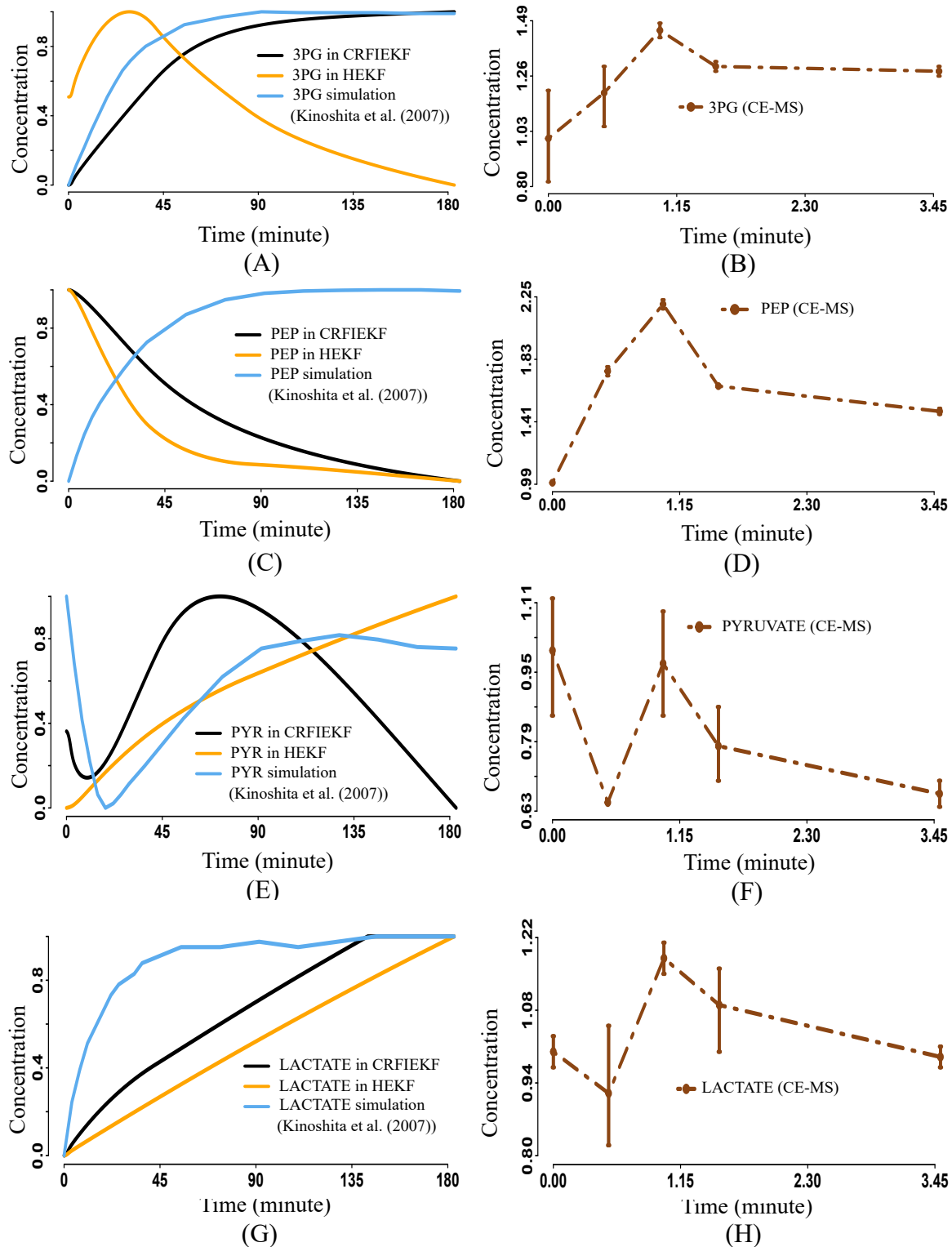


Figure 8. Validation of the proposed model during hypoxia through CE-MS measurement and simulation in human erythrocytes (Kinoshita et al. (Kinoshita et al., 2007)).

4. Parameter estimation of anaerobic glycolysis pathway in a yeast cell (Yazdani et al., 2020)

The model is depicted in Supplementary Figure 9. It comprises seven metabolites and thirteen associated kinetic parameters. The list of reactions has been presented in Supplementary Table 22. Moreover, the dynamics of the molecules have been expressed using the ordinary differential equation in Supplementary Table 23. We utilized the known approximate relationship among some of the pathway molecules to evaluate the parameter values using the proposed technique. We demonstrated such known approximate relationship in Supplementary Tables 24-25. Afterward, we revealed the dynamics of the molecules (Normalized in [0, 1]) of the pathway using the parameter values estimated by the proposed technique as well as previous investigations (Yazdani et al., 2020; Ruoff et al., 2003). The MSE (illustrated in Supplementary Table 26) between resultant concentrations of the seven metabolites by the proposed methods with time and the corresponding simulation signifies the potential of the proposed methodology.

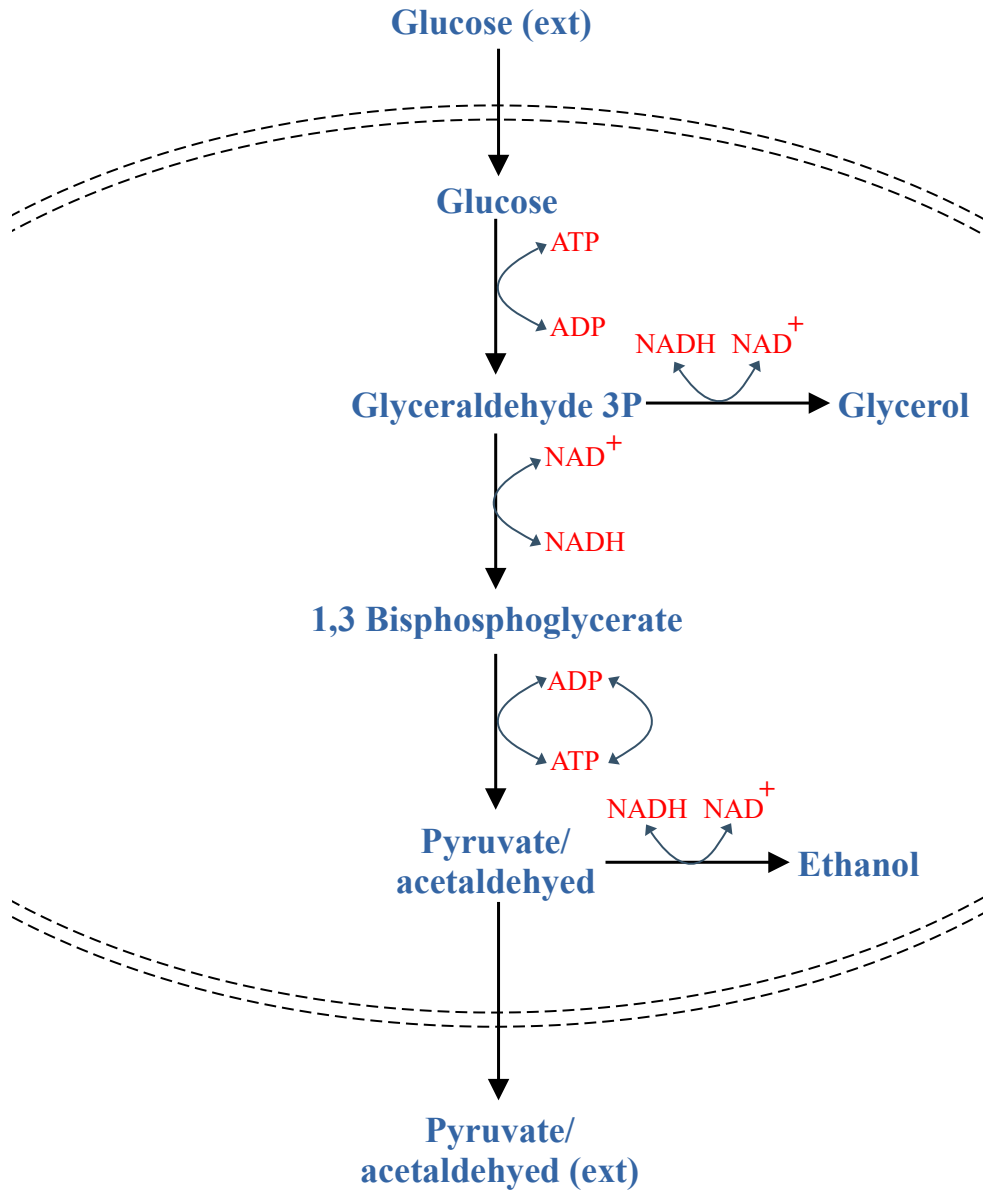


Figure 9. This figure depicts the main reactions of anaerobic glycolysis in a yeast cell (Ruoff et al., 2003) together with the influx and outflux of glucose and pyruvate/acetaldehyde, respectively.

Table 22. Reaction list contains 8 reactions of anaerobic glycolysis in a yeast cell (Ruoff et al., 2003) under consideration.

-
1. Glucose external \Rightarrow Glucose
 2. Glucose + ATP \Rightarrow Glyceraldehyde 3P + ADP
 3. Glyceraldehyde 3P + NADH \Rightarrow Glycerol + NAD⁺
 4. Glyceraldehyde 3P + NAD⁺ \Rightarrow 1,3 Bisphosphoglycerate + NADH
 5. 1,3 Bisphosphoglycerate + ADP \Rightarrow Pyruvate/acetaldehyde + ATP
 6. ATP \Rightarrow ADP
 7. Pyruvate/acetaldehyde + NADH \Rightarrow Ethanol + NAD⁺
 8. Pyruvate/acetaldehyde \Rightarrow Pyruvate/acetaldehyed (ext)
-

Table 23. It contains the list of 7 ordinary differential equations of anaerobic glycolysis in a yeast cell (Ruoff et al., 2003) under consideration.

-
1. $\frac{d\text{glucose}}{dt} = J_0 - \frac{k_1.\text{glucose}.ATP}{1+(ATP/K_1)^q}$
 2. $\frac{dglyceraldehyde3P}{dt} = 2. \frac{k_1.\text{glucose}.ATP}{1+(ATP/K_1)^q} - k_2.\text{glyceraldehyde3P}.(N - NADH) - k_6.\text{glyceraldehyde3P}.NADH$
 3. $\frac{d1,3bisphosphoglycerate}{dt} = k_2.\text{glyceraldehyde3P}.(N - NADH) - k_3.1,3bisphosphoglycerate.(A - ATP)$
 4. $\frac{dpyruvate}{dt} = k_3.1,3bisphosphoglycerate.(A - ATP) - k_4.pyruvate.NADH - \kappa.(pyruvate - pyruvate(ext))$
 5. $\frac{dNADH}{dt} = k_2.\text{glyceraldehyde3P}.(N - NADH) - k_4.pyruvate.NADH - k_6.\text{glyceraldehyde3P}.NADH$
 6. $\frac{dATP}{dt} = -2. \frac{k_1.\text{glucose}.ATP}{1+(ATP/K_1)^q} + 2.k_3.1,3bisphosphoglycerate.(A - ATP) - k_5.ATP$
 7. $\frac{dpyruvate(ext)}{dt} = \phi.\kappa.(pyruvate - pyruvate(ext)) - k.pyruvate(ext)$
-

Table 24. IF–THEN rule base for FIS to capture fuzzy relationship between glucose & glucose & ATP & glyceraldehyde

IF (glucose & ATP)		Then glyceraldehyde 3P
glucose	ATP	glyceraldehyde
LOW	LOW	LOW
LOW	MEDIUM	LOW
LOW	HIGH	LOW
MEDIUM	LOW	LOW
MEDIUM	MEDIUM	MEDIUM
MEDIUM	HIGH	MEDIUM
HIGH	LOW	MEDIUM
HIGH	MEDIUM	MEDIUM
HIGH	HIGH	HIGH

Table 25. IF–THEN rule base for FIS to capture fuzzy relationship between glucose & 1,3 bisphosphoglycerate & ATP & pyruvate

IF (1,3 bisphosphoglycerate & ATP)		Then pyruvate
1,3 bisphosphoglycerate	ATP	pyruvate
LOW	LOW	LOW
LOW	MEDIUM	LOW
LOW	HIGH	LOW
MEDIUM	LOW	LOW
MEDIUM	MEDIUM	MEDIUM
MEDIUM	HIGH	MEDIUM
HIGH	LOW	MEDIUM
HIGH	MEDIUM	MEDIUM
HIGH	HIGH	HIGH

Table 26. We employ the parameter values estimated by CRFIEKF, Ruoff et al. (Ruoff et al., 2003) and Yazdani et al. (Yazdani et al., 2020) to observe the dynamics of seven metabolites (as shown in the table) separately. Afterward, we individually evaluate two sets of MSEs representing the difference between the dynamics in the proposed technique and previous investigations (Yazdani et al., 2020; Ruoff et al., 2003). The significantly negligible MSEs of all the molecules indicate that the dynamics are indifferent in the proposed method and previous research (Yazdani et al., 2020; Ruoff et al., 2003). Such a result indicates the efficacy of the proposed technique.

Metabolite	MSE comparison	
	CRFIEKF vs Ruoff et al. (Ruoff et al., 2003)	Yazdani et al. (Yazdani et al., 2020) vs Ruoff et al. (Ruoff et al., 2003)
Glucose	0.0037	0.0001
Glyceraldehyde 3 phosphate	0.0012	0.0002
1,3-bisphosphoglycerate	0.0121	0.0001
pyruvate/acetaldehyde	0.0075	0.0001
NADH	0.0032	0.0001
ATP	0.0001	0.0004
pyruvate (external)	0.0057	0.0001

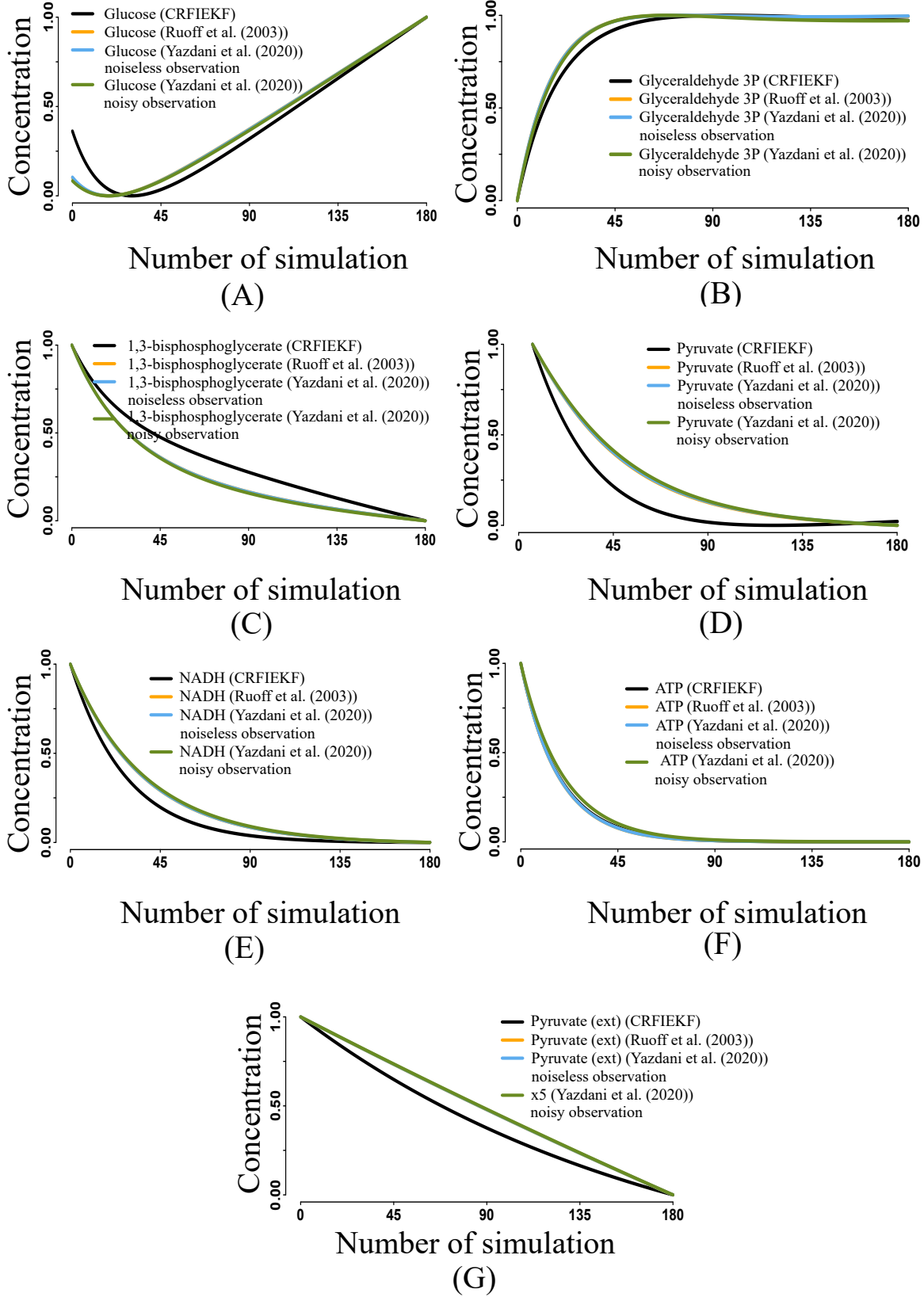


Figure 10. This figure depicts the dynamics of seven metabolites using the parameter values estimated by proposed methodology and previous investigations (Yazdani et al., 2020; Ruoff et al., 2003). Here, $x_1, x_2, x_3, x_4, x_5, x_6$ and x_7 represent Glucose, Glyceraldehyde 3P, 1,3 Bisphosphoglycerate, Pyruvate, NADH, ATP and Pyruvate external respectively.

5. Parameter estimation of JAK-STAT signal transduction pathway

The JAK/STAT (Janus kinases/signal transducers and activators of transcription) pathway is a vital signal transduction pathway that plays a pivotal role in regulating the immune response (Mertens and Darnell, 2007; Villarino et al., 2017). JAK represents a family of non-receptor tyrosine kinases in this pathway, while STAT comprises functionally related proteins. The activation process begins with the ligand erythropoietin (Epo) binding to its receptor, leading to the phosphorylation of the receptor-associated JAK. This activation, in turn, triggers the phosphorylation of monomeric STAT. Subsequently, the monomeric STAT5 is transformed into its dimeric form, which enters the nucleus to initiate the transcription of target genes. Once its active role is complete, the dimerized Stat5 undergoes dedimerization and dephosphorylation. Consequently, the dephosphorylated Stat5 is transported back to the cytoplasm. You can refer to Supplementary Figure 11 for an illustration of the JAK/STAT signal transduction pathway. A detailed list of signaling interactions, along with the equations governing the interaction fluxes, can be found in Supplementary Tables 27-29.

To represent the known approximate relationships among the molecules, we categorized them into five linguistic values: ‘low,’ ‘low-mid,’ ‘medium,’ ‘high-mid,’ and ‘high,’ considering a universe of discourse for the signal molecules within the range of [0,1]. The original parameter values, as estimated by the proposed method, along with the results from previous investigations (Sun et al., 2008; Swameye et al., 2003; Sun and Medvedovic, 2016), are presented in Supplementary Table 31. These results demonstrate the effectiveness of the proposed methodology.

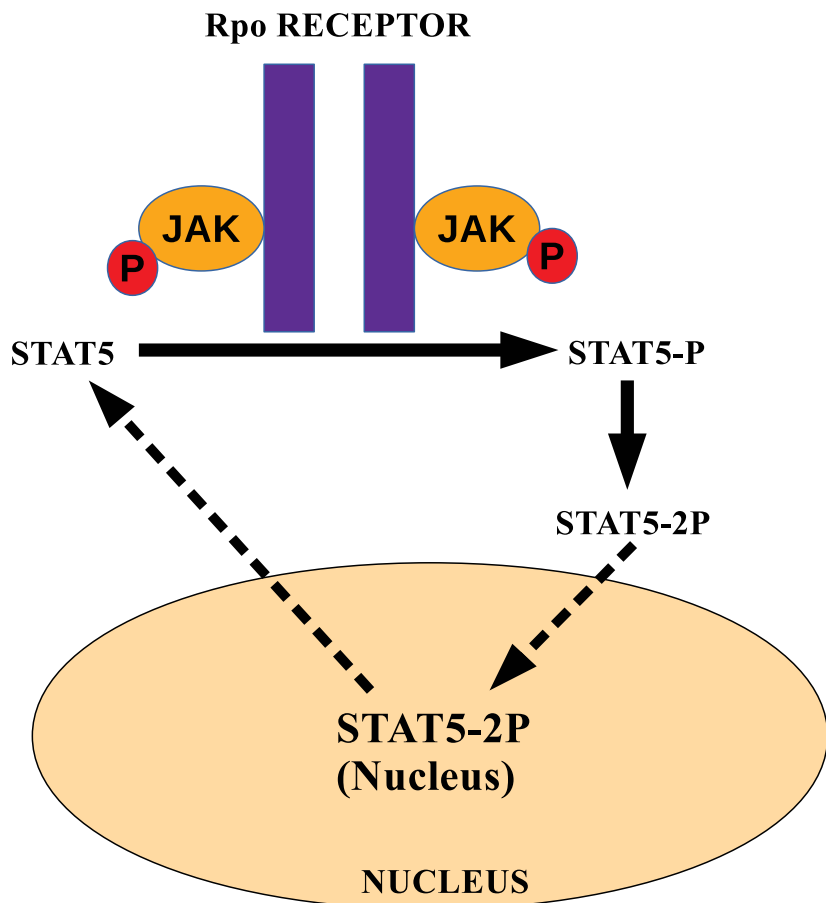


Figure 11. This figure depicts the reduced JAK/STAT signal transduction pathway under consideration.

Table 27. Reaction list contains 4 reactions from the JAK/STAT signal transduction pathway under consideration.

-
1. $EPO_R_A + STAT-5 \rightarrow STAT5-P$
 2. $2 STAT5-P \rightarrow STAT5-2P$
 3. $STAT5-2P \rightarrow STAT5-2P(NUCLEUS)$
 4. $STAT5-2P(NUCLEUS) \rightarrow 2 STAT-5$
-

Table 28. Reaction equations contains the equations of reaction fluxes associated with four reactions from the JAK/STAT signal transduction pathway under consideration.

1. $v_1 = K_1 * [STAT5] * [EPOR_A]$
2. $v_2 = K_2 * [STAT5 - P] * [STAT5 - P]$
3. $v_3 = K_3 * [STAT5 - 2P]$
4. $v_4 = K_4 * [STAT5 - 2P(NUCLEUS)]$

Table 29. It contains the stoichiometric matrix associated with four reactions from the JAK/STAT signal transduction pathway under consideration.

	v1	v2	v3	v4
STAT-5	-1	0	0	2
STAT5-P	1	-2	0	0
STAT5-2P	0	1	-1	0
STAT5-2P (NUCLEUS)	0	0	1	-1

Table 30. IF–THEN rule base for FIS to capture the fuzzy relationship between Tyrosine phosphorylated STAT5 in cytoplasm & Total STAT5 in the cytoplasm in JAK/STAT signal transduction pathway.

IF Tyrosine phosphorylated STAT5	THEN Total STAT5
Tyrosine phosphorylated STAT5	THEN Total STAT5
VERY LOW	VERY LOW
LOW	SLIGHTLY HIGH
LOW	SLIGHTLY HIGH
LOW	LOW
MEDIUM	MEDIUM
SLIGHTLY HIGH	SLIGHTLY HIGH

Table 31. This table illustrates the parameter values of JAK/STAT signal transduction pathway using the proposed method as well as previous investigations (Sun et al., 2008; Swameye et al., 2003; Sun and Medvedovic, 2016).

Kinetic Parameter	Parameter values comparison			
	Sun et. al (2008)	Swameye et al. (2003)	Sun et al. (2016)	CRFIEKF
k1	0.0211	0.021	0.022916	0.0201
k2	2.2788	2.46	2.343347	2.2003
k3	0.1064	0.1066	0.117178	0.1274
k4	0.1057	0.1066	0.102687	0.1305

6. IL6 dependent JAK-STAT3 Signal transduction pathway

IL6 plays a crucial role in regulating the inflammatory process. As depicted in Supplementary Figure 12, the mechanism of initiating IL6 signal transduction, as shown in Heinrich et al. (Heinrich, 2003), involves a series of steps. Initially, IL6 binds to its receptor subunit, glycoprotein 80 (IL6R), forming a complex. Two such complexes then bind to adaptor proteins of the glycoprotein 130 (gp130) type, resulting in the formation of a hexameric receptor complex denoted as ($R_{complex}$). Following the assembly of the receptor complex and the subsequent phosphorylation of gp130 ((p) $R_{complex}$), the signal transducer and transcription activator 3 (STAT3) protein are recruited into the phosphorylated gp130 complex. This, in turn, leads to the phosphorylation of STAT3 by the Jak protein, resulting in the formation of an active STAT3 dimer. The active STAT3 dimer influences several target genes within the nucleus, including Suppressors of Cytokine Signalling 3 (SOCS3) mRNAs and proteins. For a more detailed understanding of the interactions among these proteins, please refer to the previous investigation by Haeseler et al.(Haeseler et al., 2018).

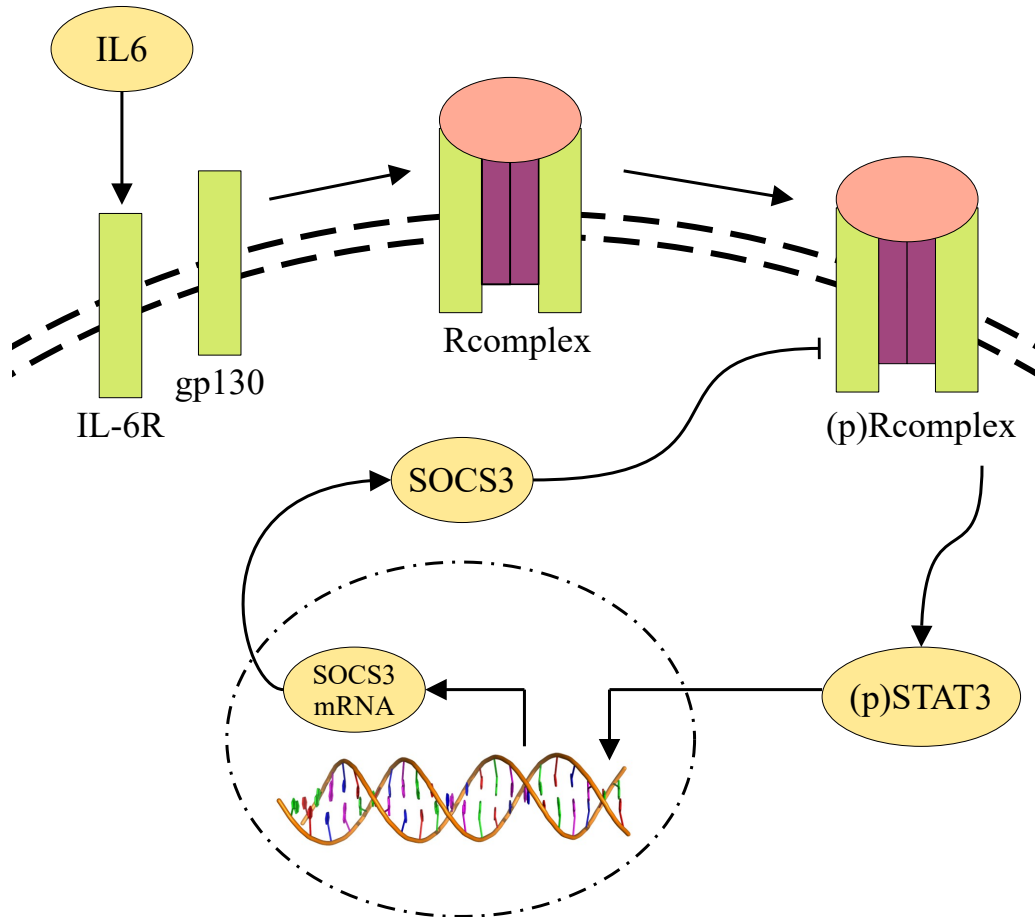


Figure 12. This figure depicts Schematic representation of IL6 dependent receptor complex assembly, Jak/STAT3 pathway activation and activation of target genes.

Table 32. Reaction ODE 5. It contains the list of 6 ordinary differential equations of IL-6-dependent Jak-STAT3 Signal transduction network (Haeseler et al., 2018) under consideration.

1. $\frac{d(IL6 - IL6R)}{dt} = p_1 \cdot IL6R \cdot IL6 - p_2 \cdot (IL6 - IL6R) - 2 \cdot p_3 \cdot (gp130)^2 \cdot (IL6 - IL6R)^2 + 2 \cdot p_4 \cdot R_{complex}$
2. $\frac{d(gp130)}{dt} = 2 \cdot p_4 \cdot R_{complex} - 2 \cdot p_3 \cdot gp130^2 \cdot (IL6 - IL6R)^2$
3. $\frac{d(p)R_{complex}}{dt} = (p_5 \cdot R_{complex}) / (1 + p_{13} \cdot (SOCS3\ protein)) - p_6 \cdot (p)R_{complex}$
4. $\frac{d(p)STAT3}{dt} = p_7 \cdot (p)R_{complex} \cdot STAT3 - p_8 \cdot (p)STAT3$
5. $\frac{d(SOCS3\ mRNA)}{dt} = p_9 \cdot (p)STAT3 - p_{10} \cdot (SOCS3\ mRNA)$
6. $\frac{d(SOCS3\ protein)}{dt} = p_{11} \cdot (SOCS3\ mRNA) - p_{12} \cdot (SOCS3\ protein)$

Table 33. IF–THEN rule base for FIS to capture fuzzy relationship between gp130 & SOCS3 protein & $(p)R_{complex}$

IF (gp130 & SOCS3 protein)		Then $(p)R_{complex}$
gp130	SOCS3 protein	$(p)R_{complex}$
LOW	LOW	LOW
LOW	MEDIUM	LOW
LOW	HIGH	LOW
MEDIUM	LOW	MEDIUM
MEDIUM	MEDIUM	MEDIUM
MEDIUM	HIGH	LOW
HIGH	LOW	HIGH
HIGH	MEDIUM	MEDIUM
HIGH	HIGH	MEDIUM

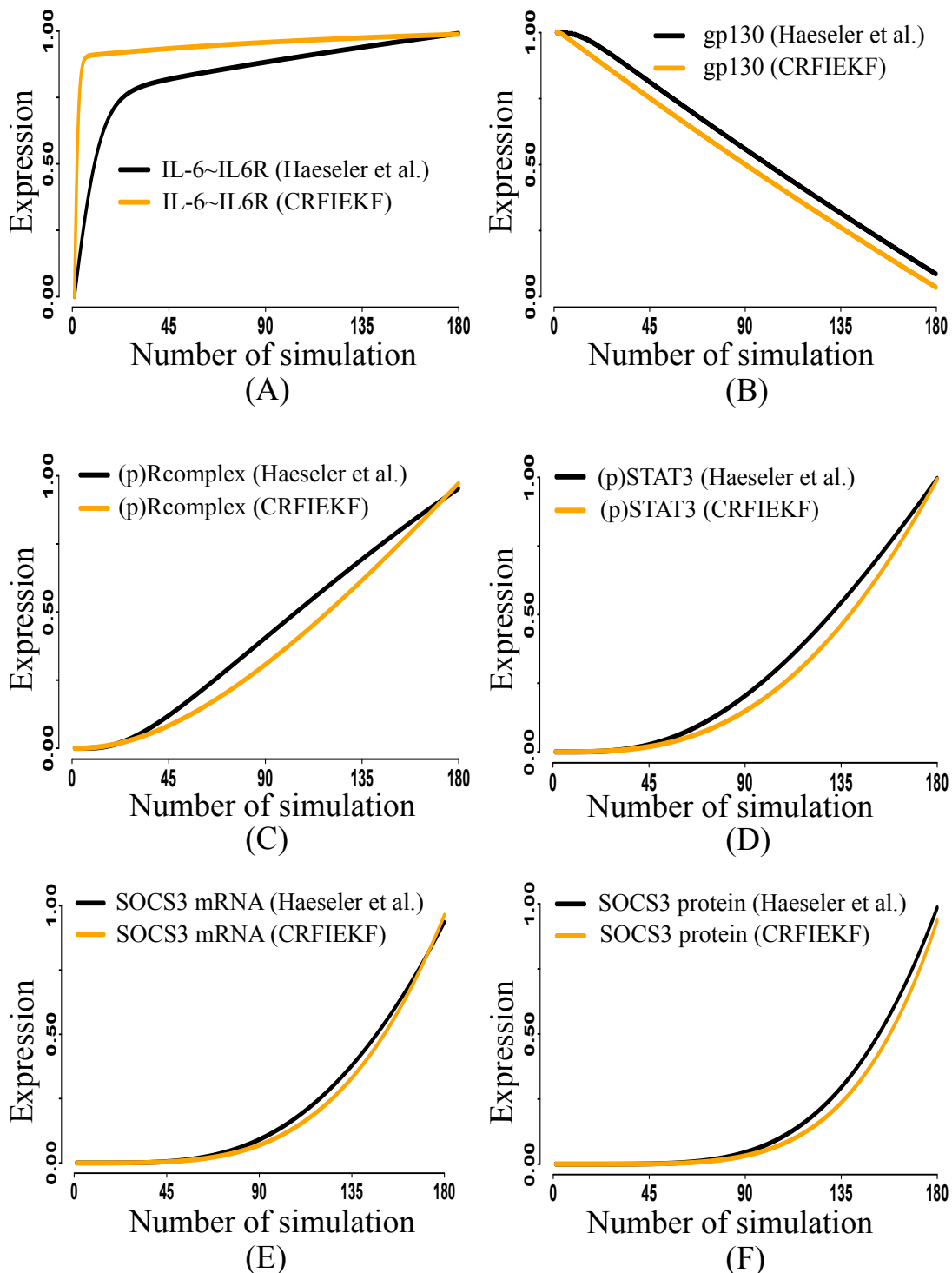


Figure 13. This figure depicts the dynamics (normalized in [0,1]) of six proteins of IL6 dependent JAK/STAT signal transduction pathway using parameter values estimated by the proposed technique and a previous investigation(Haeseler et al., 2018).

Table 34. The table illustrates the parameter values estimated by the proposed method as well as Haeseler et al.(Haeseler et al., 2018)

parameter	Proposed method	Haeseler et al.
p1	0.0100414	0.1218
p2	0.0100405	0.0388
p3	0.0100404	3.592
p4	0.0100385	0.0484
p5	0.0108882	0.0803
p6	0.0868793	0.0864
p7	0.0139551	0.156
p8	0.0100241	0.01
p9	0.010197	0.026
p10	0.0106126	0.021
p11	0.0195964	0.029
p12	0.0111405	0.008
p13	0.0854756	0.029

7. Parameter estimation of Ras/Raf/MEK/ERK signal transduction pathway

The Ras/Raf/MEK/ERK pathway is a vital mitogen-activated protein kinase (MAPK) signal transduction pathway that plays a pivotal role in controlling cell proliferation, differentiation, and survival(Kolch, 2000; Chowdhury et al., 2014). Furthermore, this cascade significantly influences apoptosis by phosphorylating various regulatory factors, including Bad, Bim, Mcl-1, and caspase-9(Li et al., 2016). While the MAPK modules share structural components, they execute diverse biological functions. Growth factor receptors can activate proto-oncogenes like Ras and Raf-1 kinase, leading to ERK activation through phosphorylation and control of targeted gene transcription. In this study, we focused on a subset of the original pathway, as detailed by Sun et al.(Sun et al., 2008) (illustrated in Supplementary Figure 14). Specifically, we considered seven reactions from the Ras/Raf/MEK/ERK signal transduction pathway. The list of signaling interactions and equations describing interaction fluxes is provided in Supplementary Tables 35 to 37.

This truncated pathway involves 11 binding rate constants. Notably, we estimated the kinetic parameters without relying on experimental observations. We developed a Fuzzy Inference System (FIS) to facilitate the estimation process to capture approximate relationships among four signaling molecules. As in previous cases, the linguistic variables in the FIS can take on three linguistic values: 'low,' 'medium,' and 'high.' Additionally, we assumed that the universe of discourse for metabolites and enzymes lies within the [0,1] range. The rule base for the FIS is detailed in Supplementary Table 38. In the subsequent analysis, we presented the original parameter values and those estimated using our proposed technique, alongside results from previous investigations(Sun et al., 2008; Kwang-Hyun et al., 2003; Capinski and Polanski, 2016), in Supplementary Table 39. We found that the sets of parameter values were statistically consistent at $p < 0.001$. Figure 5 in the original manuscript visually compares the parameter values obtained through these different techniques.

Furthermore, we used the estimated parameter values to predict the dynamics of Raf-1* and RKIP. The predicted dynamics closely matched those observed in previous investigations(Sun et al., 2008), as substantiated in Figure 6 of the original manuscript.

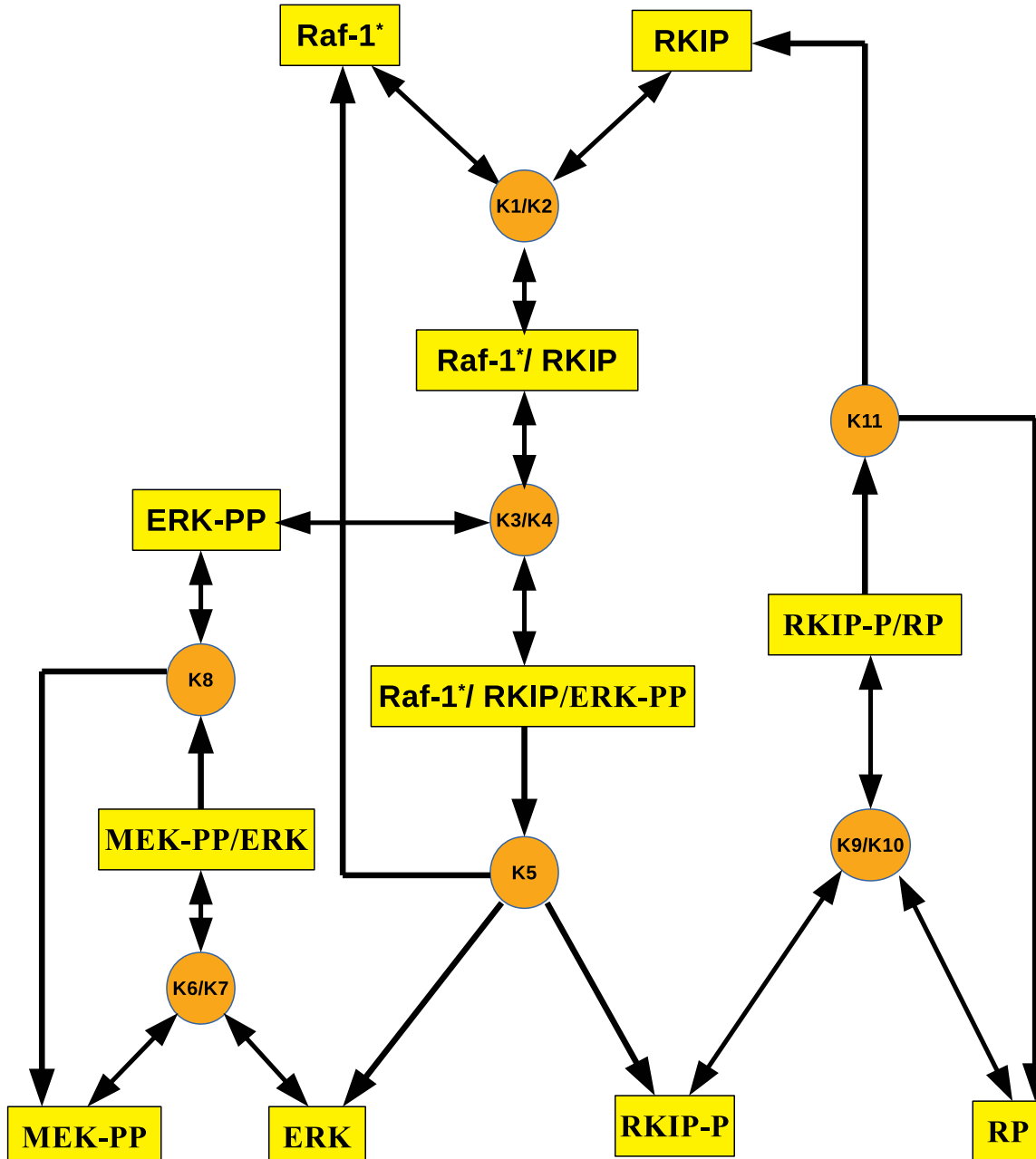


Figure 14. This figure depicts the reduced Ras/Raf/MEK/ERK signal transduction pathway under consideration.

Table 35. Reaction list contains 7 reactions from the under consideration of the Ras/Raf/MEK/ERK signal transduction pathway.

1. $\text{Raf-1}^* + \text{RKIP} \rightleftharpoons \text{Raf-1}^*/\text{RKIP}$
2. $\text{Raf1}^*/\text{RKIP} + \text{ERK-PP} \rightleftharpoons \text{Raf1}^*/\text{RKIP}/\text{ERK-PP}$
3. $\text{Raf1}^*/\text{RKIP}/\text{ERK-PP} \rightarrow \text{Raf-1}^* + \text{ERK} + \text{RKIP-P}$
4. $\text{MEK-PP} + \text{ERK} \rightleftharpoons \text{MEK-PP}/\text{ERK}$
5. $\text{MEK-PP}/\text{ERK} \rightarrow \text{MEK-PP} + \text{ERK-PP}$
6. $\text{RKIP-P} + \text{RP} \rightleftharpoons \text{RKIP-P}/\text{RP}$
7. $\text{RKIP-P}/\text{RP} \rightarrow \text{RKIP} + \text{RP}$

Table 36. Reaction equations contains the equations of reaction fluxes associated with seven reactions from the Ras/Raf/MEK/ERK signal transduction pathway under consideration.

1. $v_1 = K_1.[\text{Raf-1}^*].[RKIP-k2].[Raf-1^*/RKIP] - K_2.[\text{Raf-1}^*/RKIP]$
2. $v_2 = K_3.[\text{Raf-1}^*/\text{RKIP}].[ERK-PP-k4].[Raf-1^*/RKIP/\text{ERK-PP}] - K_4.[\text{Raf-1}^*/\text{RKIP}/\text{ERK-PP}]$
3. $v_3 = K_5.[\text{Raf-1}^*/\text{RKIP}/\text{ERK-PP}]$
4. $v_4 = K_6.[\text{ERK}].[MEK-PP-k7].[MEK-PP/\text{ERK}] - K_7.[\text{MEK-PP}/\text{ERK}]$
5. $v_5 = K_8.[\text{MEK-PP}/\text{ERK}]$
6. $v_6 = K_9.[\text{RKIP-P}].[RP]-k10.[\text{RKIP-P}/\text{RP}]$
7. $v_7 = K_{11}.[\text{RKIP-P}/\text{RP}]$

Table 37. It contains the stoichiometric matrix associated with seven reactions from the Ras/Raf/MEK/ERK signal transduction pathway under consideration.

	v1	v2	v3	v4	v5	v6	v7
Raf-1*	-1	0	1	0	0	0	0
RKIP	-1	0	0	0	0	0	1
Raf-1*/RKIP	1	-1	0	0	0	0	0
Raf-1*/RKIP/ERK-PP	0	1	-1	0	0	0	0
ERK	0	0	1	-1	0	0	0
RKIP-P	0	0	1	0	0	-1	0
MEK-PP	0	0	0	-1	1	0	0
MEK-PP/ERK	0	0	0	1	-1	0	0
ERK-PP	0	-1	0	0	1	0	0
RP	0	0	0	0	0	-1	1
RKIP-P/RP	0	0	0	0	0	1	-1

Table 38. IF–THEN rule base for FIS to capture the fuzzy relationship between MEK-PP & RP and MEK-PP/ERK & ERK-PP in Ras/Raf/MEK/ERK signal transduction pathway.

IF (MEK-PP & RP)		THEN (MEK-PP/ERK & ERK-PP)	
MEK-PP	RP	MEK-PP/ERK	ERK-PP
LOW	LOW	LOW	HIGH
LOW	MEDIUM	MEDIUM	MEDIUM
LOW	HIGH	MEDIUM	LOW
MEDIUM	LOW	HIGH	LOW
MEDIUM	MEDIUM	MEDIUM	MEDIUM
MEDIUM	HIGH	MEDIUM	LOW
HIGH	LOW	LOW	MEDIUM
HIGH	MEDIUM	HIGH	LOW
HIGH	HIGH	HIGH	LOW

Table 39. This table illustrates the parameter values of Ras/Raf/MEK/ERK signal transduction pathway using proposed method as well as previous investigations (Sun et al., 2008; Kwang-Hyun et al., 2003; Capinski and Polanski, 2016)

Kinetic Parameter	Parameter values comparison			
	Sun et. al (2008)	Kwang et al. (2003)	Capinski et al.(2016) (Classical)	CRFIEKF
k1	0.5242	0.53	0.05227	0.501
k2	0.0075	0.0072	0.0078	0.0077
k3	0.6108	0.625	0.6615	0.5907
k4	0.0025	0.00245	0.002	0.0537
k5	0.0371	0.0315	0.0312	0.0081
k6	0.8101	0.8	0.7922	0.8305
k7	0.0713	0.0075	0.0073	0.0955
k8	0.0687	0.071	0.0711	0.0594
k9	0.96	0.92	0.9207	0.9241
k10	0.0012	0.00122	0.0014	0.0033
k11	0.872	0.87	0.8622	0.7589

References

- Gengjie Jia, Gregory Stephanopoulos, and Rudiyanto Gunawan, *Incremental parameter estimation of kinetic metabolic network models*, *BMC Systems Biology*, vol. 6, no. 1, pp. 142, Springer, 2012.
- Eberhard O Voit and Jonas Almeida, *Decoupling dynamical systems for pathway identification from metabolic profiles*, *Bioinformatics*, vol. 20, no. 11, pp. 1670–1681, Oxford University Press, 2004.
- David L Nelson, Albert L Lehninger, and Michael M Cox, *Lehninger Principles of Biochemistry*, Macmillan, 2008.
- Juan P Bolaños, Angeles Almeida, and Salvador Moncada, *Glycolysis: a bioenergetic or a survival pathway?*, *Trends in Biochemical Sciences*, vol. 35, no. 3, pp. 145–149, Elsevier, 2010.
- Ayako Kinoshita, Kosuke Tsukada, Tomoyoshi Soga, Takako Hishiki, Yuki Ueno, Yoichi Nakayama, Masaru Tomita, and Makoto Suematsu, *Roles of hemoglobin allostery in hypoxia-induced metabolic alterations in erythrocytes: simulation and its verification by metabolome analysis*, *Journal of Biological Chemistry*, 2007, ASBMB.
- Gabriele Lillacci and Mustafa Khammash, *Parameter estimation and model selection in computational biology*, *PLoS Computational Biology*, vol. 6, no. 3, pp. e1000696, Public Library of Science, 2010.
- Debjyoti Paul, Abhijit Dasgupta, and Rajat K De, *Exploring the altered dynamics of mammalian central carbon metabolic pathway in cancer cells: a classical control theoretic approach*, *PloS one*, vol. 10, no. 9, pp. e0137728, Public Library of Science, 2015.
- Minoru Kanehisa and Susumu Goto, *KEGG: kyoto encyclopedia of genes and genomes*, *Nucleic acids research*, vol. 28, no. 1, pp. 27–30, Oxford University Press, 2000.
- Alireza Yazdani, Lu Lu, Maziar Raissi, and George Em Karniadakis, *Systems biology informed deep learning for inferring parameters and hidden dynamics*, *PLoS Computational Biology*, vol. 16, no. 11, pp. e1007575, Public Library of Science, 2020.
- Peter Ruoff, Melinda K Christensen, Jana Wolf, and Reinhart Heinrich, *Temperature dependency and temperature compensation in a model of yeast glycolytic oscillations*, *Biophysical Chemistry*, vol. 106, no. 2, pp. 179–192, Elsevier, 2003.
- Claudia Mertens and James E Darnell, *Snapshot: Jak-stat signaling*, *Cell*, vol. 131, no. 3, pp. 612, Elsevier, 2007.
- Alejandro V Villarino, Yuka Kanno, and John J O'Shea, *Mechanisms and consequences of Jak-STAT signaling in the immune system*, *Nature Immunology*, vol. 18, no. 4, pp. 374, Nature Publishing Group, 2017.
- Xiaodian Sun, Li Jin, and Momiao Xiong, *Extended Kalman filter for estimation of parameters in nonlinear state-space models of biochemical networks*, *PloS One*, vol. 3, no. 11, pp. e3758, Public Library of Science, 2008.
- Ira Swameye, TG Müller, Jens Timmer, O Sandra, and Ursula Klingmüller, *Identification of nucleocytoplasmic cycling as a remote sensor in cellular signaling by databased modeling*, *Proceedings of the National Academy of Sciences*, vol. 100, no. 3, pp. 1028–1033, National Acad Sciences, 2003.
- Xiaodian Sun and Mario Medvedovic, *Model reduction and parameter estimation of non-linear dynamical biochemical reaction networks*, *IET Systems Biology*, vol. 10, no. 1, pp. 10–16, IET, 2016.
- PC Heinrich, *Principles of interleukin (IL)-6-type cytokine signalling and its regulation*, *Biochem J*, vol. 374, pp. 1–20, 2003.
- Friedrich v Haeseler, Nadine Rudolph, Rolf Findeisen, and Heinrich J Huber, *Parameter Estimation for Signal Transduction Networks from Experimental Time Series Using Picard Iteration*, *IFAC-PapersOnLine*, vol. 51, no. 18, pp. 191–196, Elsevier, 2018.
- Walter Kolch, *Meaningful relationships: the regulation of the Ras/Raf/MEK/ERK pathway by protein interactions*, *Biochemical Journal*, vol. 351, no. 2, pp. 289–305, Portland Press Limited, 2000.
- Indrajit Chowdhury, Winston E Thompson, and Kelwyn Thomas, *Prohibitins role in cellular survival through Ras-Raf-MEK-ERK pathway*, *Journal of Cellular Physiology*, vol. 229, no. 8, pp. 998–1004, Wiley Online Library, 2014.
- Lei Li, Guo-Dong Zhao, Zhe Shi, Li-Li Qi, Li-Yuan Zhou, and Ze-Xian Fu, *The Ras/Raf/MEK/ERK signaling pathway and its role in the occurrence and development of HCC*, *Oncology Letters*, vol. 12, no. 5, pp. 3045–3050, Spandidos Publications, 2016.
- Cho Kwang-Hyun, Shin Sung-Young, Kim Hyun-Woo, Olaf Wolkenhauer, Brian McFerran, and Walter Kolch, *Mathematical modeling of the influence of RKIP on the ERK signaling pathway*, in *International Conference on Computational Methods in Systems Biology*, pp. 127–141, Springer, 2003.
- Michał Capinski and Andrzej Polanski, *Parameter Estimation in Systems Biology Models by Using Extended Kalman Filter*, in *Man-Machine Interactions 4*, pp. 195–204, Springer, 2016.